2011

Development, verification and experimental analysis of high-fidelity mathematical models for control moment gyros

McManus, Christine D.

Monterey, California : Naval Postgraduate School

NAVAL POSTGRADUATE SCHOOL

MONTEREY, CALIFORNIA

THESIS

DEVELOPMENT, VERIFICATION AND EXPERIMENTAL ANALYSIS OF HIGH-FIDELITY MATHEMATICAL MODELS FOR CONTROL MOMENT GYROS

by

Christine D. McManus

December 2011

Thesis Advisor: I. Michael Ross
Second Reader: James H. Newman

Approved for public release; distribution is unlimited

THIS PAGE INTENTIONALLY LEFT BLANK

REPORT DOCUMENTATION PAGE		Form Approved OMB No. 0704-0188

Public reporting burden for this collection of information is estimated to average 1 hour per response, including the time for reviewing instruction, searching existing data sources, gathering and maintaining the data needed, and completing and reviewing the collection of information. Send comments regarding this burden estimate or any other aspect of this collection of information, including suggestions for reducing this burden, to Washington headquarters Services, Directorate for Information Operations and Reports, 1215 Jefferson Davis Highway, Suite 1204, Arlington, VA 22202-4302, and to the Office of Management and Budget, Paperwork Reduction Project (0704-0188) Washington DC 20503.

1. AGENCY USE ONLY *(Leave blank)*	2. REPORT DATE December 2011	3. REPORT TYPE AND DATES COVERED Master's Thesis
4. TITLE AND SUBTITLE Development, Verification and Experimental Analysis of High-Fidelity Mathematical Models for Control Moment Gyros		**5. FUNDING NUMBERS**
6. AUTHOR(S) Christine D. McManus		
7. PERFORMING ORGANIZATION NAME(S) AND ADDRESS(ES) Naval Postgraduate School Monterey, CA 93943-5000		**8. PERFORMING ORGANIZATION REPORT NUMBER**
9. SPONSORING /MONITORING AGENCY NAME(S) AND ADDRESS(ES) N/A		**10. SPONSORING/MONITORING AGENCY REPORT NUMBER**

11. SUPPLEMENTARY NOTES The views expressed in this thesis are those of the author and do not reflect the official policy or position of the Department of Defense or the U.S. Government. I.R. B. Protocol number ___N.A.__.

12a. DISTRIBUTION / AVAILABILITY STATEMENT Approved for public release; distribution is unlimited	12b. DISTRIBUTION CODE

13. ABSTRACT (maximum 200 words)

In the operation of CMGs there exists a concept called "back drive," which represents a case where the coupling effects of the angular velocity of the body and the angular momentum of the CMG overwhelm the input torque and result in a lack of control. This effect is known but not well documented or studied in the literature.

Starting from first principles, this thesis derives the full nonlinear dynamical equations for CMGs. These equations contain significantly more terms than are found in the literature. As a means to understand the implications of these terms, a reduced order model is derived. The full and reduced models are then validated by means of extensive simulations. Finally, experimental verification of the models confirms the finding that the reduced order model provides a reasonably high fidelity for dynamics.

14. SUBJECT TERMS Control Moment Gyroscope, dynamics, high-fidelity mathematical model			15. NUMBER OF PAGES 93
			16. PRICE CODE
17. SECURITY CLASSIFICATION OF REPORT Unclassified	18. SECURITY CLASSIFICATION OF THIS PAGE Unclassified	19. SECURITY CLASSIFICATION OF ABSTRACT Unclassified	20. LIMITATION OF ABSTRACT UU

NSN 7540-01-280-5500

Standard Form 298 (Rev. 2-89)
Prescribed by ANSI Std. 239-18

THIS PAGE INTENTIONALLY LEFT BLANK

DEVELOPMENT, VERIFICATION AND EXPERIMENTAL ANALYSIS OF HIGH-FIDELITY MATHEMATICAL MODELS FOR CONTROL MOMENT GYROS

Christine D. McManus
Commander, United States Navy
B.S., Massachusetts Institute of Technology, 1995

Submitted in partial fulfillment of the
requirements for the degree of

MASTER OF SCIENCE IN ASTRONAUTICAL ENGINEERING

from the

**NAVAL POSTGRADUATE SCHOOL
December 2011**

Author: Christine D. McManus

Approved by: I. Michael Ross
                   Thesis Advisor

                   James H. Newman
                   Second Reader

                   Knox T. Millsaps
                   Chair, Department of Mechanical and Aerospace Engineering

THIS PAGE INTENTIONALLY LEFT BLANK

ABSTRACT

In the operation of CMGs there exists a concept called "back drive," which represents a case where the coupling effects of the angular velocity of the body and the angular momentum of the CMG overwhelm the input torque and result in a lack of control. This effect is known but not well documented or studied in the literature.

Starting from first principles, this thesis derives the full nonlinear dynamical equations for CMGs. These equations contain significantly more terms than are found in the literature. As a means to understand the implications of these terms, a reduced order model is derived. The full and reduced models are then validated by means of extensive simulations. Finally, experimental verification of the models confirms the finding that the reduced order model provides a reasonably high fidelity for dynamics.

THIS PAGE INTENTIONALLY LEFT BLANK

TABLE OF CONTENTS

LIST OF FIGURES

\

LIST OF TABLES

THIS PAGE INTENTIONALLY LEFT BLANK

NOMENCLATURE

Latin Variables		Greek Variables	
DCM	Direction Cosine Matrix	δ	Gimbal angle
h, **h**	Angular Momentum (unbolded indicated scalar, bold indicates vector)	Ω	Angular velocity of the rotor
J	Moment of Inertia Tensor (subscripts indicate specific MOIs, numerical subscripts indicate referenced axis, i.e., $\mathbf{J_r}$ is the full rotor MOI; J_{r_1} is the scalar value of the rotor MOI about the 1 axis)	ω, $\boldsymbol{\omega}$	Angular velocity of the body (unbolded indicated scalar, bold indicates vector)
t, **t**	Torque (unbolded indicates scalar, bold indicates vector)		

Subscripts		Frames of Reference	
r	Rotor	r	Rotor
g	Gimbal	g	Gimbal
b	Body	b	Body
1, 2, 3	Axis	N	Inertial
		sys	System

THIS PAGE INTENTIONALLY LEFT BLANK

ACKNOWLEDGMENTS

The author would like to thank the following for their invaluable assistance in the completion of this thesis:

Dr. I. Michael Ross for his expertise and guidance throughout the thesis process.

Dr. James H. Newman for his invaluable work as second reader – this thesis was greatly improved as a result.

Dr. Mark Karpenko for his wealth of knowledge, advice, and hours of patient discussion.

My classmates and friends whose help, advice and humor helped get us all through to the end.

My mother, Kathleen M. Minton, my stepfather, CAPT David C. Minton III, USN, RET, my sister, Elizabeth D. McManus and my nephew, William D. Hutcheson for their advice, patience, love, encouragement, and constant support which has made my work possible.

And above all, my father, LT Floyd L. McManus, USN, RET, who encouraged me to be curious about the world and believed that nothing was beyond my reach.

THIS PAGE INTENTIONALLY LEFT BLANK

I. INTRODUCTION

In the study of Control Moment Gyroscopes (CMGs) there exists a concept called "back drive," which represents a case where the coupling effects of the angular velocity of the body and the angular momentum of the CMG overwhelm the input torque and result in a lack of control. This effect is known in industry but not well documented or studied in the literature.

The standard model of a spacecraft with Control Moment Gyroscopes used by most textbooks and papers assumes that the control variable of the CMG is the CMG gimbal rate. In this model the complete angular momentum $(\mathbf{h})$ of a single CMG is assumed to be the moment of inertia of the rotor multiplied by the angular velocity of the rotation about the spin axis, shown in Equation (1) where J_{r_1} is the rotor inertia, Ω is the rotor angular velocity and $\hat{g}_1$ is the spin axis of the CMG, as shown in Figure 1.

$$\mathbf{h} = J_{r_1}\Omega\hat{g}_1 \qquad (1)$$
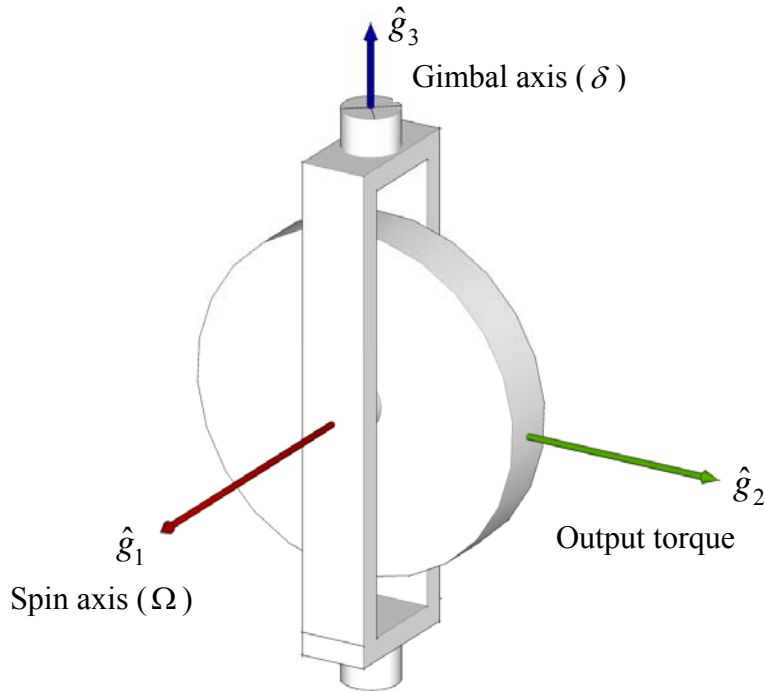
Figure 1.   Schematic of CMG and nomenclature.

The angular momentum of a system of n-CMGs in the body frame, which will be fully derived in Section IV but is useful now, is then defined as Equation (2) where $h_0 = J_r\Omega$, δ is the gimbal angle, β is the pyramid skew angle and ϕ is the rotation angle due to the placement of the CMGs as shown in Figure 2.

$$\mathbf{h}\hat{b} = \sum_{i=1}^{n} h_0 \begin{bmatrix} c\delta_i c\phi_i - s\delta_i c\beta s\phi_i \\ c\delta_i s\phi_i + s\delta_i c\beta c\phi_i \\ s\delta_i s\beta \end{bmatrix} \tag{2}$$

where $c\delta \equiv \cos(\delta)$, $\quad s\delta \equiv \sin(\delta)$, $\quad c\phi \equiv \cos(\phi)$, $s\phi \equiv \sin(\phi)$ $\quad$, $c\beta \equiv \cos(\beta)$, $\quad$ and $s\beta \equiv \sin(\beta)$.

A typical n=4 system is shown in Figure 2 as an example of the geometry. The angles β, ϕ and δ are labeled on representative CMGs but are not labeled where their inclusion would reduce the clarity of the figure. The axes labeled $\hat{b}_1, \hat{b}_2$, and $\hat{b}_3$ constitute the satellite reference frame.
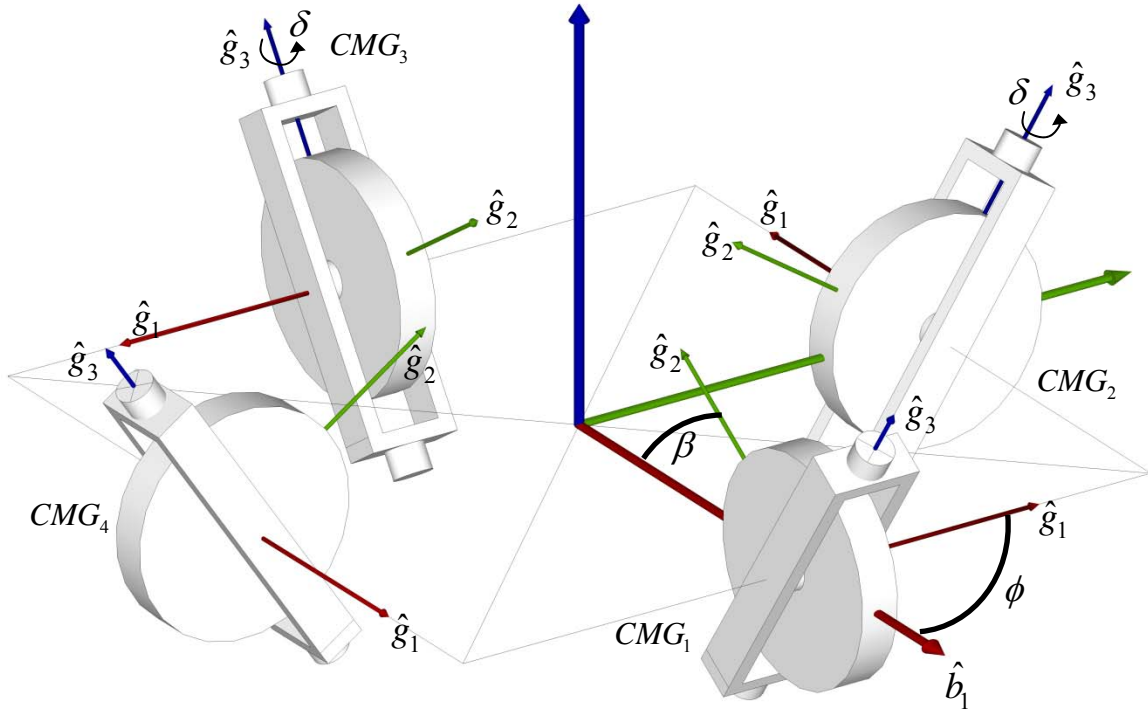
Figure 2. A typical n=4 CMG Pyramid. Both ϕ (offset) and β (skew) angles are fixed, determined by the mounting of the CMGs with respect to the spacecraft reference frame ($\hat{b}_1, \hat{b}_2, \hat{b}_3$).

With the angular momentum defined as in Equation (2), for any given CMG h_0, β, and ϕ are all constant in time and δ is the only time varying component. Therefore the derivative can be expressed as:

$$\dot{\mathbf{h}} = h_0 \sum_{i=1}^{n} \frac{\partial}{\partial \delta} \left(\begin{bmatrix} c\delta_i c\phi_i - s\delta_i c\beta s\phi_i \\ c\delta_i s\phi_i + s\delta_i c\beta c\phi_i \\ s\delta_i s\beta \end{bmatrix} \right) \dot{\delta}_i \qquad (3)$$

If we define:

$$\mathbf{a}_i = h_0 \frac{\partial}{\partial \delta} \left(\begin{bmatrix} c\delta_i c\phi_i - s\delta_i c\beta s\phi_i \\ c\delta_i s\phi_i + s\delta_i c\beta c\phi_i \\ s\delta_i s\beta \end{bmatrix} \right) \tag{4}$$

Then:

$$\dot{\mathbf{h}} = \begin{bmatrix} \mathbf{a}_1 & \cdots & \mathbf{a}_n \end{bmatrix} \begin{bmatrix} \dot{\delta}_1 \\ \vdots \\ \dot{\delta}_n \end{bmatrix} = \mathbf{A}\dot{\boldsymbol{\delta}} \tag{5}$$

At a system level, the rotational equation of motion of a spacecraft with a CMG system is given as Equation (6) where $\mathbf{h}_{sys}$ is the angular momentum of the entire spacecraft-CMG system.

$$\mathbf{t}_{ext} = \dot{\mathbf{h}}_{sys} + \boldsymbol{\omega} \times \mathbf{h}_{sys} \tag{6}$$

Because angular momentum is conserved we can write the angular momentum of the system as the sum of the angular momentum of the spacecraft body and the angular momentum of the CMG system as shown in Equation (7).

$$\mathbf{h}_{sys} = \mathbf{h}_b + \mathbf{h}_{CMG} = \mathbf{J}_b \boldsymbol{\omega}^{b/N} + \mathbf{h}_{CMG} \tag{7}$$

where $\mathbf{J}_b$ is the inertia matrix of the spacecraft and $\boldsymbol{\omega}$ is the angular velocity of the spacecraft expressed in the body frame ($\hat{b}$ in Figure 2). Combining Equations (6) and (7) results in:

$$\mathbf{t}_{ext} = \mathbf{J}_b \dot{\boldsymbol{\omega}}^{b/N} + \dot{\mathbf{h}}_{CMG} + \boldsymbol{\omega}^{b/N} \times \left(\mathbf{J}_b \boldsymbol{\omega}^{b/N} + \mathbf{h}_{CMG} \right) \tag{8}$$

By defining the internal control torque generated by the CMG system as:

$$\mathbf{u} = -\left(\dot{\mathbf{h}}_{CMG} + \boldsymbol{\omega}^{b/N} \times \mathbf{h}_{CMG} \right) \tag{9}$$

We obtain:

$$\mathbf{t}_{ext} + \mathbf{u} = \mathbf{J}_b \dot{\boldsymbol{\omega}}^{b/N} + \boldsymbol{\omega}^{b/N} \times \mathbf{J}_b \boldsymbol{\omega}^{b/N} \tag{10}$$

Combining Equations (9) and (5) the gimbal rate can be obtained as

$$\dot{\boldsymbol{\delta}} = \mathbf{A}^{-1} \left(-\mathbf{u} - \boldsymbol{\omega}^{b/N} \times \mathbf{h}_{CMG} \right) \tag{11}$$

4

Equation (11) is only valid for $n = 3$, therefore a more general approach uses the pseudo-inverse shown in Equation (12) to obtain the commanded gimbal rate.

$$\dot{\boldsymbol{\delta}} = \left(\mathbf{A}^T \left(\mathbf{A}\mathbf{A}^T\right)^{-1}\right)\left(-\mathbf{u} - \boldsymbol{\omega}^{b/N} \times \mathbf{h}_{CMG}\right) \tag{12}$$

This results in the state space equations in Equation (13).

$$\dot{\mathbf{q}} = \frac{1}{2}\left(\boldsymbol{\omega}^*\mathbf{q}\right)$$

$$\dot{\boldsymbol{\omega}} = \mathbf{J}_b^{-1}\left(\left(\mathbf{t}_{ext} + \mathbf{u}\right) - \left(\boldsymbol{\omega}^{b/N} \times \mathbf{J}_b\boldsymbol{\omega}^{b/N}\right)\right) \tag{13}$$

$$\dot{\boldsymbol{\delta}} = \left(\mathbf{A}^T \left(\mathbf{A}\mathbf{A}^T\right)^{-1}\right)\left(-\mathbf{u} - \boldsymbol{\omega}^{b/N} \times \mathbf{h}_{CMG}\right)$$

Where $\boldsymbol{\omega}^*$ is defined as:

$$\boldsymbol{\omega}^* \equiv \begin{bmatrix} 0 & \omega_3 & -\omega_2 & \omega_1 \\ -\omega_3 & 0 & \omega_1 & \omega_2 \\ \omega_2 & -\omega_1 & 0 & \omega_3 \\ -\omega_1 & -\omega_2 & -\omega_3 & 0 \end{bmatrix} \tag{14}$$

This 7+n state space model is sufficient for many applications, but using this technique serves to mask the inner dynamics of the CMG. Figure 3 shows many of the intricacies of the inner dynamics of a CMG, which are neglected in the analysis shown above.
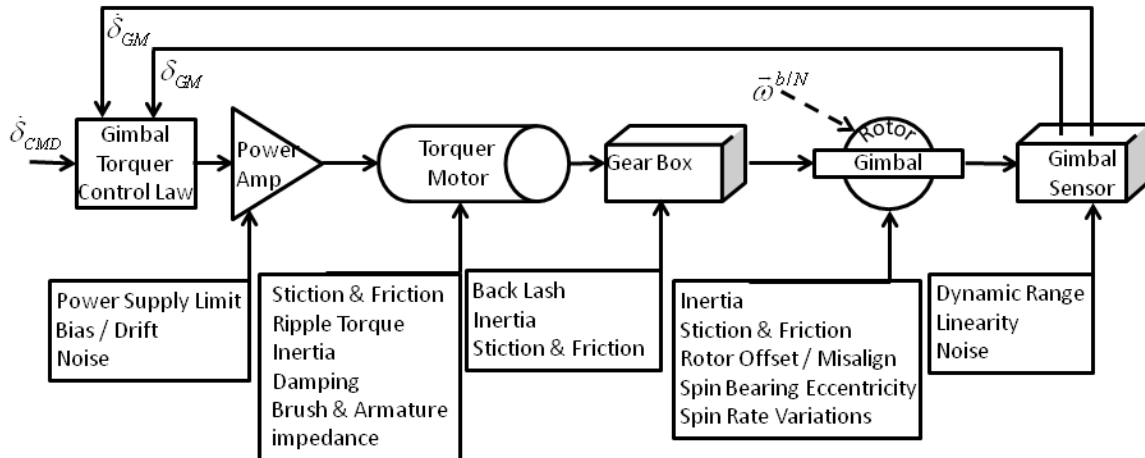
Figure 3.　　CMG Inner Loop. After Leonard.[1]

5

In the physical world, the control variable for the CMG is the motor current of the CMG gimbal motor. Approaching the problem from this perspective increases the complexity significantly and the relationship between motor current and gimbal torque can be considered fairly well known. Therefore a better analysis of the spacecraft/CMG system can be conducted using the gimbal torque as the control variable. To accomplish this, the system must be analyzed using the detailed dynamics of the CMG-spacecraft system.

This thesis includes a summary of past and current literature on the dynamics of CMG clusters with emphasis on derivations of the equations of motion and the implications of the gimbal torque equations, followed by a detailed derivation of the dynamics. The full equations of motion are modeled and, using simulation and experimental data, the physical implications of the equations are determined and discussed.

Section Notes

1 Barry S. Leonard, Control Moment Gyro Systems, Vol. AE3818 Lecture Notes (Monterey, CA: , 2002).

THIS PAGE INTENTIONALLY LEFT BLANK

II.   LITERATURE REVIEW

A.   MOTIVATION

Much research has been conducted on Control Moment Gyroscope controlled satellites since they were first developed in the 1950s.[1-13]   However, limited published research can be found on the detailed derivation of the full dynamics of CMGs and of the derivations that exist, none could be found that discuss the physical implications. Searches of several databases, including the American Institute of Aeronautics and Astronautics (AIAA) and the National Aeronautics and Space Administration (NASA) document server, revealed a series of trends in the publically available published research.

Early research in the 1960s and early 1970s focused on the basic issues of using CMGs in space—many specifically focusing on SKYLAB.[2,3,4,5]   This research occasionally included a detailed derivation of the dynamics of a CMG/spacecraft system but the developed equations do not appear to drive CMG design.[6]   Once the research on the SKYLAB system was completed, there appears to be a gap in publically available research on the dynamics of CMGs throughout the remainder of the 1970s and 1980s.

There are a scattering of papers in the 1970s and 1980s, primarily focused on using CMGs for fine pointing of space telescopes.[7]   These papers are largely focused on hardware design and steering law refinements.[8,9,10]   The dynamics of the CMG were not a primary focus of this research and the published hardware design research does not emphasize gimbal torque requirements.

The 1990s and early 2000s seemed to see a resurgence of CMG dynamics research, much of it focused on either precision attitude control of spacecraft or in the relatively new field of using CMGs in robotics.[11,12,13,14]   A great deal of the robotics research focuses on scissored pair CMG systems, which involve some unique dynamics of their own.[15]

An overview of the published research is included.

9

B.   EARLY LITERATURE

CMG analysis and research in the 1960s varied widely. However, several papers include a derivation of the dynamics of a CMG system. Havill and Ratcliff(1964)[16] derive the equations of motion of an ideal single degree of freedom CMG in their paper regarding twin-gyro attitude control systems but as their proposed system cancels the motor torque by design, they do not go into depth on the topic. The equation they develop for gimbal torque is shown in Equation (15).

$$t_{CMG_3} = \left(J_{g_3} + J_{r_3} \right) \left[\dot{\omega}_3 + \ddot{\delta} \right] - J_{r_1} \Omega \omega_{g_2} \tag{15}$$

This equation neglects terms created by the body rate coupling but includes the rest of what appear to be the commonly accepted terms.

Liska and Jacot (1966)[17] derive the dynamic equations for a linearized simple CMG in their paper on the use of CMGs and reaction jets for manned space station attitude control. They use a simplified derivation to find the gimbal torque shown in Equation (16).

$$t_{CMG_3} - D\dot{\delta} + J_{r_1} \Omega \omega_{g_2} = \left(J_{g_3} + J_{r_3} \right) \ddot{\delta} \tag{16}$$

This equation includes a drag component but does not include the body rate cross product term and the input from the spacecraft acceleration. Liska and Jacot state that they are neglecting "as insignificant those torques caused by rotation of the small gimbal mass at vehicle rates."

Schindelin (1968)[18] did not explicitly derive an equation for gimbal torque in his paper *On Space Vehicle Attitude Stabilization by Passive Control Moment Gyros* but did derive the equations of motion of the CMG about the gimbal axis which, due to the passive nature of the system, was set to zero. Shown in Equation (17) the equation is effectively Equation (16) without specifically including the drag terms.

$$0 = \left(J_{g_3} + J_{r_3} \right) \ddot{\delta} + J_{r_1} \Omega \omega_{g_2} \tag{17}$$

These papers are the only ones of the era that could be found that included any discussion of the gimbal torque motor and all derived the gimbal torque equation as a tangent to their major purpose. None were found that specified the assumptions made to develop their versions of the equations.

C.   MODERN LITERATURE

Published papers in the 1970s and 1980s focused primarily on steering and control law improvements. A number of NASA papers were also published that contained descriptions of the hardware for specific CMG systems, although nothing was found that detailed decision design drivers.[19,20]

During the 1990s, most research continued to focus on steering law improvements, with an emphasis on time optimal reorientations, including research that proved that an Eigenaxis maneuver was not time optimal in all cases.[21] The late 1990s and early 2000s also resulted in a number of papers on the possibility of miniaturizing CMGs for use in small spacecraft.[22,23,24] Notably, Busseuil, et al. published a paper in 1998, which actually discusses gimbal motor sizing for miniaturized CMGs.[25] However, they begin with the assumptions in Equation (18) and do not explicitly address the derivation of the equations of motion or what terms they are neglecting.

$$t_{CMG_3} = \left(J_{g_3} + J_{r_3} \right) \ddot{\delta} + J_{r_1} \Omega \omega_{g_2}$$
$$t_{CMG_2} = J_{r_1} \Omega \left(\omega_{g_3} + \dot{\delta} \right)$$

(18)

From Equation (18) they derive the required maximum torque required from the gimbal motor as shown in Equation (19).

$$t_{CMG_2}^{MAX} = \left(J_{g_3} + J_{r_3} \right) \ddot{\delta}^{MAX} + J_{r_1} \Omega \omega_{g_2}^{MAX}$$

(19)

This is the only paper that was found that explicitly states an equation for sizing a CMG gimbal motor.

Many papers of this era use Equation (18) as a baseline assumption, without addressing the simplifications made. In this thesis these equations will be known as the Reduced Model.

11

D. DYNAMICS TEXTBOOKS

The majority of current dynamics textbooks include a fairly straightforward derivation and discussion of the use of CMGs as a momentum management system but generally fail to delve deeply into the internal dynamics of the CMG system, focusing, reasonably, on the issues of singularity avoidance. In *Analytical Mechanics of Aerospace Systems*, Schaub and Junkins, [26] include a derivation of the rotational equations of motion for a system with a single Variable Speed CMG (VSCMG), then expand it to an N-VSCMGs system. This derivation is in support of an argument for using Variable Speed Control Moment Gyroscopes for singularity avoidance. They derive the resultant torque of movement of the CMG rotor as Equation (20).

$$
\begin{aligned}
\mathbf{\dot{h}}_r &= \hat{g}_2 J_{r_2} \left(\dot{\Omega} + \hat{g}_1^T \dot{\omega} + \dot{\delta}\omega_2 \right) \\
&+ \hat{g}_1 \left(J_{r_1}\dot{\delta}\omega_2 + J_{r_1}\hat{g}_1^T \dot{\omega} + \omega_2\omega_3 \left(J_{r_2} - J_{r_3} \right) + J_{r_2}\Omega\left(\dot{\delta} + \omega_3\right) - 2J_{r_1}\dot{\delta}\omega_2 \right) \\
&+ \hat{g}_3 \left(J_{r_1}\left(\hat{g}_3^T \dot{\omega} + \ddot{\delta} \right) + \left(\omega_1\omega_2 \left(J_{r_1} - J_{r_2} \right) \right) - J_{r_2}\Omega\omega_1 \right)
\end{aligned}
\tag{20}
$$

As the CMG gimbal motor operates only in the gimbal axis, the motor torque is shown in Equation (21).

$$
t_g = \left(J_{r_1}\left(\hat{g}_3^T \dot{\omega} + \ddot{\delta} \right) + \left(\omega_1\omega_2 \left(J_{r_1} - J_{r_2} \right) \right) - J_{r_2}\Omega\omega_1 \right)
\tag{21}
$$

The derivation included in this document confirms the equations that Schaub and Junkins developed. The approaches used in the two derivations are sufficiently different that a high degree of confidence in the resultant equations is justified.

Section Notes

2 Arthur D. Jacot and Donald J. Liska, "Control Moment Gyros in Attitude Control." Journal of Spacecraft and Rockets (August, 1966), 1313-1320.

3 H. B. Kennedy, "Gyro Momentum Exchange Device for Space Vehicle Attitude Control," AIAA Journal 1, no. 5 (May, 1963), 1110.

4 Hans F. Kennel, "Skylab Attitude Control and Angular Momentum Desaturation with One Double-Gimbaled Control Moment Gyro," NASA Technical Memorandum X- 64746 (1973).

5 L. A. Morine and B. J. O'Connor, "A Description of the CMG and its Application to Space Vehicle Control." (AIAA Guidance, Control And Flight Dynamics Conference, Huntsville, AL, August 14-16, 1969).

6 Jerry R. Havill and Jack W. Ratcliff, "A Twin-Gyro Attitude Control System for Space Vehicles," NASA Technical Note D-2419 (August, 1964).

7 Frederick R. Morrell, "An Investigation of the Fine-Pointing Control System of a Soft Gimbaled Orbiting Telescope." NASA Technical Note D-5829 (1970).

8 H. S. Oh and S. R. Vadali, "Maneuvering Strategies using CMGs" (Goddard Flight Mechanics/Estimation Theory Symposium, Space Flight Center, Greenbelt, MD, May 10-11, 1988).

9 Bong Wie, "Quaternion Feedback for Spacecraft Large Angle Maneuvers," Journal of Guidance, Control and Dynamics 8, no. 3 (May-June 1985, 1985), 360-365.

10 Bong Wie, "Quarternion Feedback Regulator for Spacecraft Eigenaxis Rotations," Journal of Guidance, Control, and Dynamics 12 (May-June, 1989), 375.

11 Karl D. Bilimoria and Bong Wie, "Time-Optimal Three-Axis Reorientation of a Rigid Spacecraft," Journal of Guidance Control Dynamics 16 (1993), 452.

12 Jacques Busseuil, Michel Llibre and Xavier Roser, "High Precision Mini-CMG's and their Spacecraft Applications" (Advances in the Astronautical Sciences-Guidance and Control, Breckenridge, CO, February 4-8, 1998).

13 Jiuqing Wan and Jiuqing Yu, "High Precision Satellite Attitude Control Based on Feedforward Compensation" (The Sixth World Congress on Intelligent Control and Automation, Dalian, China, June 21–23, 2006).

14 H. Yoon and P. Tsiotras, "Spacecraft Adaptive Attitude and Power Tracking with Variable Speed Control Moment Gyroscopes," *Journal of Guidance Control and Dynamics* 25, no. 6 (2002), 1081.

15 Stephanie J. Thomas, Michael A. Paluszek and Mason Peck, "Architecture for Low-Power, High-Agility Multibody Control" (AIAA Infotech@Aerospace, Arlington, VA, September 26-28, 2005).

16 Jerry R. Havill and Jack W. Ratcliff, "A Twin-Gyro Attitude Control System for Space Vehicles," NASA Technical Note D-2419 (August, 1964).

17 Arthur D. Jacot and Donald J. Liska, "Control Moment Gyros in Attitude Control." Journal of Spacecraft and Rockets (August, 1966), 1313-1320.

18 J. W. Schindelin, "On Space Vehicle Attitude Stabilization by Passive Control Moment Gyros," NASA Contractor Report #100280 (June, 1968).

19 P. R. Burke and P. A. Coronato, "A Gimbal Sizing Analysis for an IPACS Rotating Assembly," NASA Contractor Report #172524 (March, 1985).

20 J. M. Kolvek, "Advanced Control Moment Gyro Development [Final Summary Report]," NASA Contractor Report #120567 (1974).

21 Karl D. Bilimoria and Bong Wie, "Time-Optimal Three-Axis Reorientation of a Rigid Spacecraft," Journal of Guidance Control Dynamics 16 (1993), 452.

22 Porter Davis, "Momentum System Concepts and Trades for the New Class of Smaller Lower Cost Satellites," Advances in the Astronautical Sciences 125 (2006), 13-24.

23 V. Lappas, W. H. Steyn and C. Underwood, "Design and Testing of a Control Moment Gyroscope Cluster for Small Satellites," Journal of Spacecraft and Rockets 42, no. 4 (July-Aug., 2005), 729-739.

24 Frederick Leve, Andrew Tatsch and Norman Fitz-Coy, "A Scalable Control Moment Gyro Design for Attitude Control of Micro-, Nano-, and Pico-Class Satellites," Advances in the Astronautical Sciences Guidance and Control 2007 127 (2007), 235.

25 Jacques Busseuil, Michel Llibre and Xavier Roser, "High Precision Mini-CMG's and their Spacecraft Applications" (Advances in the Astronautical Sciences-Guidance and Control, Breckenridge, CO, February 4-8, 1998).

26 Hanspeter Schaub and John L. Junkins, Analytical Mechanics of Space Systems (Reston, VA: American Institute of Aeronautics and Astronautics, 2003), 141.

III. DEVELOPMENT OF HIGH-FIDELITY MATHEMATICAL MODELS FOR A SINGLE CMG SYSTEM

A. RIGID BODY DYNAMICS

For a general system, the rigid body state equations can be derived as shown in Equation (22).[27]

$$\dot{q}_1 = \frac{1}{2}\left(q_4\omega_1 - \left(q_3\omega_2 - q_2\omega_3\right)\right)$$

$$\dot{q}_2 = \frac{1}{2}\left(q_4\omega_2 - \left(q_1\omega_3 - q_3\omega_1\right)\right)$$

$$\dot{q}_3 = \frac{1}{2}\left(q_4\omega_3 - \left(q_2\omega_1 - q_1\omega_2\right)\right)$$

$$\dot{q}_4 = -\frac{1}{2}\left(q_1\omega_1 + q_2\omega_2 + q_3\omega_3\right) \tag{22}$$

$$\dot{\omega}_1 = \frac{1}{J_1}\left(t_1 + \left(J_3 - J_2\right)\omega_2\omega_3\right)$$

$$\dot{\omega}_2 = \frac{1}{J_2}\left(t_2 + \left(J_1 - J_3\right)\omega_1\omega_3\right)$$

$$\dot{\omega}_3 = \frac{1}{J_3}\left(t_3 + \left(J_2 - J_1\right)\omega_1\omega_2\right)$$

This system assumes that the applied torque (T_i) is external to the system. In the case of CMG controlled spacecraft, this assumption is not valid due to the complex coupling effects of the system.

B. SYSTEM DEFINITION

A CMG controlled spacecraft system has four frames of reference: the inertial frame, the body frame, the gimbal frame and the rotor frame. Figure 4 shows a diagram of a CMG with the gimbal and rotor frames labeled. By definition, $\hat{r}_1$ and $\hat{g}_1$ are collinear.
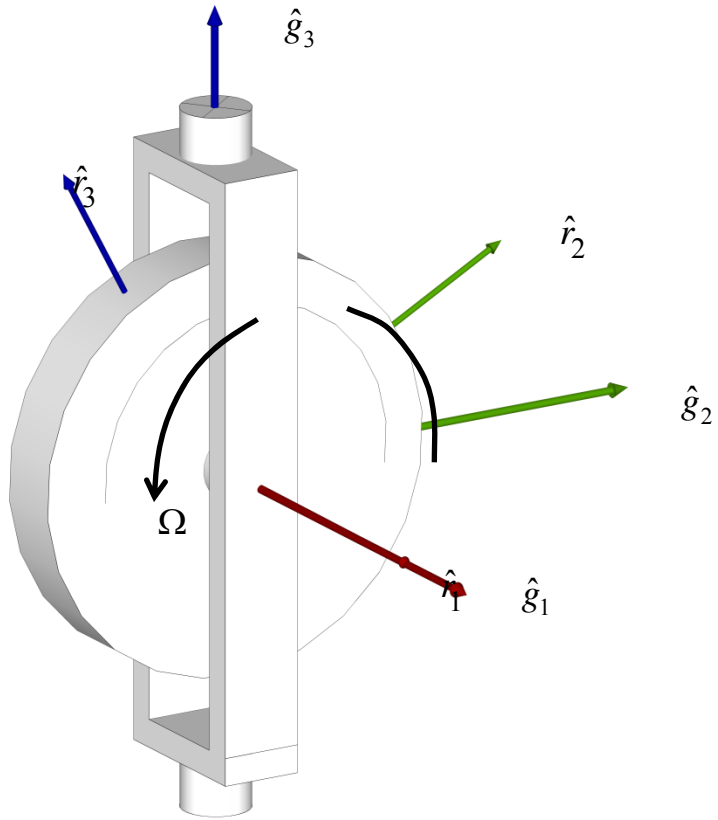
Figure 4.   CMG diagram showing the gimbal and rotor frames of reference.

Figure 5 shows a system diagram with all the frames of reference labeled.
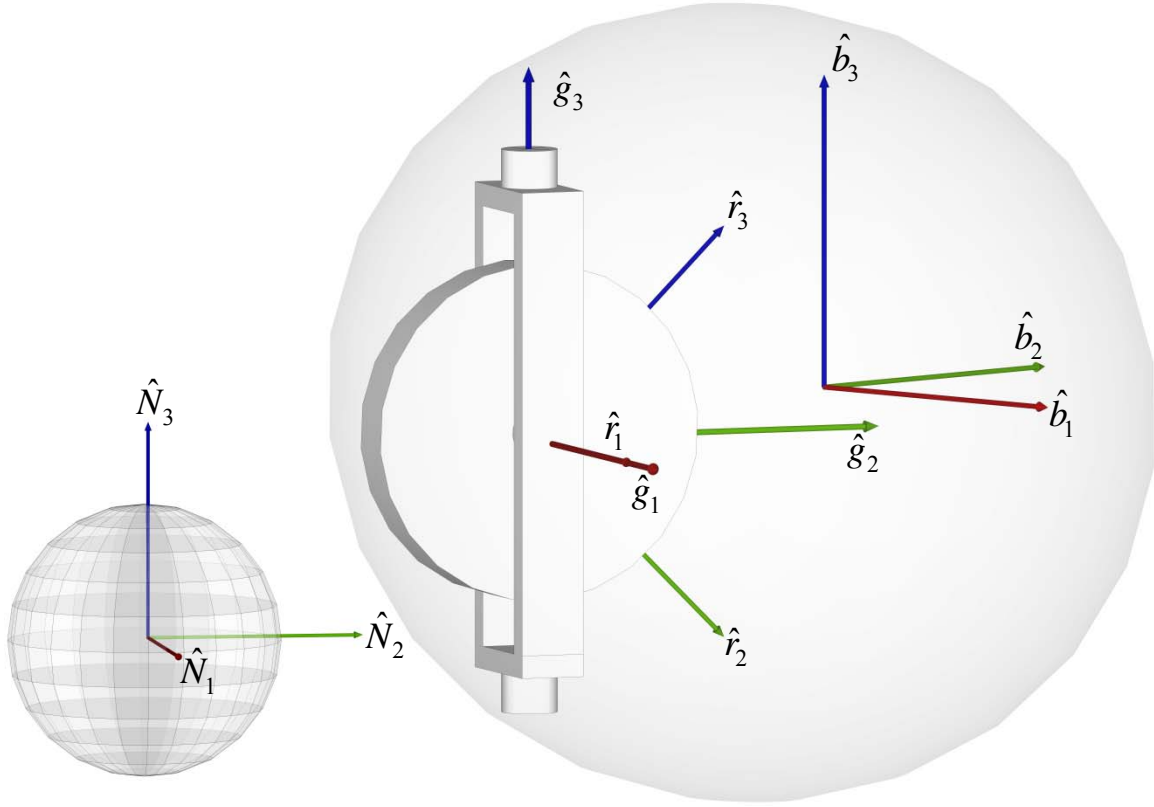
Figure 5.   System diagram with the gimbal, rotor, body and inertial frames of reference.

For the following derivation, subscripts identify which frame and, when appropriate, which axis the component is reference to. Superscripts for angular velocity note the rotation frames of reference, for instance $\vec{\omega}^{b/N}$ indicates the rotation of the body with respect to the inertial frame. A single superscript used with a derivative term indicates the frame in which the derivative is taken, for instance $\left(\dfrac{d\left(\boldsymbol{\omega}^{b/N}\right)}{dt}\right)^{g}$ indicates the derivative of the rotation of the body with respect to the inertial frame, taken in the gimbal frame. Each frame is rotating with respect to its mounting frame.

Therefore, the angular momentum of the system can be written as Equation (23).

$$\mathbf{h}_{tot} = \mathbf{h}_{b} + \mathbf{h}_{g} + \mathbf{h}_{r} \tag{23}$$

By definition any change in the angular momentum of the system is the result of external torque applied to the system, shown in Equation (24).

$$\mathbf{t}_{ext} = \left(\frac{d\mathbf{h}_{tot}}{dt} \right)^N \tag{24}$$

If the external torque is known we can solve for $\dot{\omega}$ for the system, which can then be used to solve the system dynamics.

With the assumption of rigid attachment, we also assume that the rotation of the CMG gimbal and rotor are perfectly aligned and can be defined as:

$$\omega^{r/g} = \Omega \hat{r}_1 \qquad \omega^{g/b} = \dot{\delta} \hat{g}_3 \tag{25}$$

The inertia dyads for each component of the system are defined as shown in Equation (26).

$$\mathbf{J}_b = \begin{bmatrix} J_{b_1} & 0 & 0 \\ 0 & J_{b_2} & 0 \\ 0 & 0 & J_{b_3} \end{bmatrix} \qquad \mathbf{J}_g = \begin{bmatrix} J_{g_1} & 0 & 0 \\ 0 & J_{g_2} & 0 \\ 0 & 0 & J_{g_3} \end{bmatrix} \qquad \mathbf{J}_r = \begin{bmatrix} J_{r_1} & 0 & 0 \\ 0 & J_{r_2} & 0 \\ 0 & 0 & J_{r_3} \end{bmatrix} \tag{26}$$

The angular momentum of each component is therefore:

$$\mathbf{h}_b = \mathbf{J}_b \cdot \omega^{b/N} \qquad \mathbf{h}_g = \mathbf{J}_g \cdot \omega^{g/N} \qquad \mathbf{h}_r = \mathbf{J}_r \cdot \omega^{r/N} \tag{27}$$

From the addition theorem of angular velocity, we can show that the angular velocity of the gimbal and the rotor in the inertial frame are equal to the sum of their angular velocities in each applicable frame:

$$\omega^{g/N} = \omega^{b/N} + \omega^{g/b}; \qquad \omega^{r/N} = \omega^{b/N} + \omega^{g/b} + \omega^{r/g} \tag{28}$$

For the purposes of the initial single CMG derivation, we assume that the body frame and the gimbal frame are initially aligned and that the only variation between the two frames takes place about the gimbal axis. Therefore, the Direction Cosine Matrix between the gimbal and the body frame can be defined as:

18

$$\mathbf{DCM}^{g/b} = \mathbf{C}^{g/b} = \begin{bmatrix} \cos(\delta) & \sin(\delta) & 0 \\ -\sin(\delta) & \cos(\delta) & 0 \\ 0 & 0 & 1 \end{bmatrix} \qquad (29)$$

We then define then angular velocity of the body frame in the inertial frame as:

$$\boldsymbol{\omega}^{b/N} = \begin{bmatrix} \omega_1 \\ \omega_2 \\ \omega_3 \end{bmatrix} \qquad (30)$$

$\boldsymbol{\omega}^{b/N}$ can then be transformed to the gimbal frame as shown in Equation (31). $\boldsymbol{\omega}^{b_g/N}$ is defined as the angular velocity of the spacecraft in the body frame translated into the gimbal frame. This step is necessary for future calculations in the gimbal frame.

$$\boldsymbol{\omega}^{b_g/N} = \begin{bmatrix} \cos(\delta) & \sin(\delta) & 0 \\ -\sin(\delta) & \cos(\delta) & 0 \\ 0 & 0 & 1 \end{bmatrix} \begin{bmatrix} \omega_1 \\ \omega_2 \\ \omega_3 \end{bmatrix} = \begin{bmatrix} \omega_1 \cos(\delta) + \omega_2 \sin(\delta) \\ -\omega_1 \sin(\delta) + \omega_2 \cos(\delta) \\ \omega_3 \end{bmatrix} \hat{g} \equiv \begin{bmatrix} \omega_{g_1} \\ \omega_{g_2} \\ \omega_{g_3} \end{bmatrix} \hat{g} \quad (31)$$

With these definitions in place we can separate the angular momentum of each component and take the derivative in the inertial frame in order to determine the overall system $\dot{\omega}$ the inertial frame.

C.   EQUATIONS OF MOTION FOR THE BODY

As defined in Equation (27), the angular momentum of the body is:

$$\mathbf{h}_b = \mathbf{J}_b \boldsymbol{\omega}^{b/N} \qquad (32)$$

where all terms are defined in the body frame. Using the transport theorem, the derivative of H_b in the inertial frame is:

$$\begin{aligned} \left(\frac{d\mathbf{h}_b}{dt} \right)^N &= \left(\frac{d\mathbf{h}_b}{dt} \right)^b + \boldsymbol{\omega}^{b/N} \times \mathbf{h}_b \\ &= \mathbf{J}_b \left[\dot{\boldsymbol{\omega}}^{b/N} \right]^b + \boldsymbol{\omega}^{b/N} \times \mathbf{J}_b \boldsymbol{\omega}^{b/N} \end{aligned} \qquad (33)$$

As expected, leaving all terms in the body frame and taking the cross product results in the original equations for a rigid body system.

19

$$t_{b_1} = \left[J_{b_1} \dot{\omega}_1 \right]^b + \left[\left(J_{b_3} - J_{b_2} \right) \omega_2 \omega_3 \right] \hat{b}_1$$

$$t_{b_2} = \left[J_{b_2} \dot{\omega}_2 \right]^b + \left[\left(J_{b_1} - J_{b_3} \right) \omega_1 \omega_3 \right] \hat{b}_2 \tag{34}$$

$$t_{b_3} = \left[J_{b_3} \dot{\omega}_3 \right]^b + \left[\left(J_{b_2} - J_{b_1} \right) \omega_1 \omega_2 \right] \hat{b}_3$$

D.   EQUATIONS OF MOTION FOR THE GIMBAL

As defined in Equation (27), the angular momentum of the gimbal is:

$$\mathbf{h}_g = \mathbf{J}_g \boldsymbol{\omega}^{g/N} \tag{35}$$

In this case, both $\mathbf{J}_g$ and $\boldsymbol{\omega}^{g/N}$ are defined in the gimbal frame.   Using the transport theorem the inertial derivative is:

$$\left(\frac{d\mathbf{h}_g}{dt} \right)^N = \left(\frac{d\mathbf{h}_g}{dt} \right)^g + \boldsymbol{\omega}^{g/N} \times \mathbf{h}_g$$

$$= \left(\frac{d\left(\mathbf{J}_g \boldsymbol{\omega}^{g/N} \right)}{dt} \right)^g + \boldsymbol{\omega}^{g/N} \times \mathbf{J}_g \mathbf{h}^{g/N} \tag{36}$$

Substituting $\boldsymbol{\omega}^{g/N}$ from Equation (28) in results in:

$$\left(\frac{d\mathbf{h}_g}{dt} \right)^N = \left(\frac{d\left(\mathbf{J}_g \left(\boldsymbol{\omega}^{b/N} + \boldsymbol{\omega}^{g/b} \right) \right)}{dt} \right)^g + \left(\boldsymbol{\omega}^{b/N} + \boldsymbol{\omega}^{g/b} \right) \times \mathbf{J}_g \left(\boldsymbol{\omega}^{b/N} + \boldsymbol{\omega}^{g/b} \right) \tag{37}$$

Expanding the terms, Equation (37) becomes:

$$\left(\frac{d\mathbf{h}_g}{dt} \right)^N = \left(\frac{d\left(\mathbf{J}_g \boldsymbol{\omega}^{b/N} \right)}{dt} \right)^g + \left(\frac{d\left(\mathbf{J}_g \boldsymbol{\omega}^{g/b} \right)}{dt} \right)^g$$

$$+ \boldsymbol{\omega}^{b/N} \times \mathbf{J}_g \boldsymbol{\omega}^{b/N} + \boldsymbol{\omega}^{g/b} \times \mathbf{J}_g \boldsymbol{\omega}^{b/N} \tag{38}$$

$$+ \boldsymbol{\omega}^{b/N} \times \mathbf{J}_g \boldsymbol{\omega}^{g/b} + \boldsymbol{\omega}^{g/b} \times \mathbf{J}_g \boldsymbol{\omega}^{g/b}$$

For clarity, each of the six terms will be evaluated separately.

1.   Gimbal Term 1

Because $\mathbf{J}_g$ is constant in the gimbal frame, it can be removed from the derivative. Then, the transport theorem is used to shift back into the body frame, which results in:

$$\left(\frac{d\left(\mathbf{J}_g\boldsymbol{\omega}^{b/N}\right)}{dt}\right)^g = \mathbf{J}_g\left(\frac{d\left(\boldsymbol{\omega}^{b/N}\right)}{dt}\right)^g$$

$$= \mathbf{J}_g\left(\left(\frac{d\left(\boldsymbol{\omega}^{b/N}\right)}{dt}\right)^b + \boldsymbol{\omega}^{b/g}\times\boldsymbol{\omega}^{b/N}\right) \tag{39}$$

In order to take the cross product of $\boldsymbol{\omega}^{b/g}$ and $\boldsymbol{\omega}^{b/N}$ we recognize that $\boldsymbol{\omega}^{b/g}$ is equivalent to $-\boldsymbol{\omega}^{g/b}$, which was defined in Equation (25) and that both vectors need to be in the same frame of reference, therefore we need to use $\boldsymbol{\omega}^{b_g/N}$ as defined in Equation (31). This results in Equation (40).

$$\left(\frac{d\left(\mathbf{J}_g\boldsymbol{\omega}^{b/N}\right)}{dt}\right)^g = \begin{bmatrix} J_{g_1} & 0 & 0 \\ 0 & J_{g_2} & 0 \\ 0 & 0 & J_{g_3} \end{bmatrix}\left(\begin{bmatrix} \dot{\omega}_1 \\ \dot{\omega}_2 \\ \dot{\omega}_3 \end{bmatrix}\hat{b} + \begin{bmatrix} 0 \\ 0 \\ -\dot{\delta} \end{bmatrix}\hat{g} \times \begin{bmatrix} \omega_{g_1} \\ \omega_{g_2} \\ \omega_{g_3} \end{bmatrix}\hat{g}\right)$$

$$= \begin{bmatrix} J_{g_1}\dot{\omega}_1 \\ J_{g_2}\dot{\omega}_2 \\ J_{g_3}\dot{\omega}_3 \end{bmatrix}\hat{b} + \begin{bmatrix} J_{g_1}\dot{\delta}\omega_{g_2} \\ -J_{g_2}\dot{\delta}\omega_{g_1} \\ 0 \end{bmatrix}\hat{g} \tag{40}$$

2.   Gimbal Term 2

Again, $\mathbf{J}_g$ is removed from the derivative and because $\boldsymbol{\omega}^{g/b}$ is defined in the gimbal frame the result is simply:

$$\mathbf{J}_g\left(\frac{d\left(\boldsymbol{\omega}^{g/b}\right)}{dt}\right)^g = \begin{bmatrix} 0 \\ 0 \\ J_{g_3}\ddot{\delta} \end{bmatrix}\hat{g} \tag{41}$$

3.   Gimbal Term 3

As in term 1, we use $\boldsymbol{\omega}^{b_g/N}$ and take the cross product:

21

$$\boldsymbol{\omega}^{b_g/N} \times \mathbf{J}_g \boldsymbol{\omega}^{b_g/N} = \begin{bmatrix} \omega_{g_1} \\ \omega_{g_2} \\ \omega_{g_3} \end{bmatrix} \times \begin{bmatrix} J_{g_1}\omega_{g_1} \\ J_{g_2}\omega_{g_2} \\ J_{g_3}\omega_{g_3} \end{bmatrix}$$

$$= \begin{bmatrix} \omega_{2_g}\omega_{3_g}\left(J_{g_3} - J_{g_2}\right) \\ \omega_{1_g}\omega_{3_g}\left(J_{g_1} - J_{g_3}\right) \\ \omega_{1_g}\omega_{2_g}\left(J_{g_2} - J_{g_1}\right) \end{bmatrix} \tag{42}$$

4.   Gimbal Term 4

We use $\boldsymbol{\omega}^{g/b}$ and $\boldsymbol{\omega}^{b_g/N}$ in the gimbal frame and take the cross product:

$$\boldsymbol{\omega}^{g/b} \times \mathbf{J}_g \boldsymbol{\omega}^{b/N} = \dot{\delta}\hat{g}_3 \times \mathbf{J}_g \boldsymbol{\omega}^{b/N}$$

$$= \begin{bmatrix} 0 \\ 0 \\ \dot{\delta} \end{bmatrix} \times \begin{bmatrix} J_{g_1}\omega_{g_1} \\ J_{g_2}\omega_{g_2} \\ J_{g_3}\omega_{g_3} \end{bmatrix} \tag{43}$$

$$= \begin{bmatrix} -J_{g_2}\dot{\delta}\omega_{g_2} \\ J_{g_1}\dot{\delta}\omega_{g_1} \\ 0 \end{bmatrix} \hat{g}$$

5.   Gimbal Term 5

We use $\boldsymbol{\omega}^{b_g/N}$ and $\boldsymbol{\omega}^{g/b}$ in the gimbal frame and take the cross product:

$$\boldsymbol{\omega}^{b/N} \times \mathbf{J}_g \boldsymbol{\omega}^{g/b} = \boldsymbol{\omega}^{b/N} \times \mathbf{J}_g \dot{\delta} \hat{g}_1$$

$$= \begin{bmatrix} \omega_{g_1} \\ \omega_{g_2} \\ \omega_{g_3} \end{bmatrix} \times \begin{bmatrix} 0 \\ 0 \\ J_{g_3} \dot{\delta} \end{bmatrix} \tag{44}$$

$$= \begin{bmatrix} J_{g_3} \dot{\delta} \omega_{g_2} \\ -J_{g_3} \dot{\delta} \omega_{g_1} \\ 0 \end{bmatrix} \hat{g}$$

6. Gimbal Term 6

$\boldsymbol{\omega}^{g/b}$ is crossed with the scalar multiple of itself and is therefore zero:

$$\boldsymbol{\omega}^{g/b} \times \mathbf{J}_g \boldsymbol{\omega}^{g/b} = \dot{\delta} \hat{g}_1 \times \mathbf{J}_g \dot{\delta} \hat{g}_1$$

$$= \begin{bmatrix} 0 \\ 0 \\ \dot{\delta} \end{bmatrix} \times \begin{bmatrix} 0 \\ 0 \\ J_{g_3} \dot{\delta} \end{bmatrix} = 0 \tag{45}$$

These terms can be combined and grouped for the following result for torque resulting from the motion of the gimbal shown in Equation (46).

$$\mathbf{t}_g = \begin{bmatrix} J_{g_1} \dot{\omega}_1 \\ J_{g_2} \dot{\omega}_2 \\ J_{g_3} \dot{\omega}_3 \end{bmatrix} \hat{b} + \begin{bmatrix} J_{g_1} \dot{\delta} \omega_{g_2} \\ -J_{g_2} \dot{\delta} \omega_{g_1} \\ 0 \end{bmatrix} \hat{g} + \begin{bmatrix} 0 \\ 0 \\ J_{g_3} \ddot{\delta} \end{bmatrix} \hat{g} + \begin{bmatrix} \omega_{2_g} \omega_{3_g} \left(J_{g_3} - J_{g_2} \right) \\ \omega_{1_g} \omega_{3_g} \left(J_{g_1} - J_{g_3} \right) \\ \omega_{1_g} \omega_{2_g} \left(J_{g_2} - J_{g_1} \right) \end{bmatrix} \hat{g}$$

$$+ \begin{bmatrix} -J_{g_2} \dot{\delta} \omega_{g_2} \\ J_{g_1} \dot{\delta} \omega_{g_1} \\ 0 \end{bmatrix} \hat{g} + \begin{bmatrix} J_{g_3} \dot{\delta} \omega_{g_2} \\ -J_{g_3} \dot{\delta} \omega_{g_1} \\ 0 \end{bmatrix} \hat{g} \tag{46}$$

E. EQUATIONS OF MOTION FOR THE ROTOR

As defined in Equation (27), the angular momentum of the rotor is:

$$\mathbf{h}_r = \mathbf{J}_r \boldsymbol{\omega}^{r/N} \tag{47}$$

Because we assume the wheel is symmetric about $\hat{r}_1$, which is collinear with $\hat{g}_1$, we can define both $\mathbf{J}_r$ and $\boldsymbol{\omega}^{r/N}$ in the gimbal frame. Again, using the transport theorem the inertial derivative is:

$$\left(\frac{d\mathbf{h}_r}{dt}\right)^N = \left(\frac{d\mathbf{h}_r}{dt}\right)^g + \boldsymbol{\omega}^{r/N} \times \mathbf{h}_r$$

$$= \left(\frac{d\left(\mathbf{J}_r\boldsymbol{\omega}^{r/N}\right)}{dt}\right)^g + \boldsymbol{\omega}^{r/N} \times \mathbf{J}_g\boldsymbol{\omega}^{r/N} \tag{48}$$

Substituting $\boldsymbol{\omega}^{r/N}$ from Equation (28) includes the following nine terms:

$$\left(\frac{d\mathbf{h}_r}{dt}\right)^N = \left(\frac{d\left(\mathbf{J}_r\left(\boldsymbol{\omega}^{b/N} + \boldsymbol{\omega}^{g/b} + \boldsymbol{\omega}^{r/g}\right)\right)}{dt}\right)^g + \left(\boldsymbol{\omega}^{b/N} + \boldsymbol{\omega}^{g/b} + \boldsymbol{\omega}^{r/g}\right) \times \mathbf{J}_r\left(\boldsymbol{\omega}^{b/N} + \boldsymbol{\omega}^{g/b} + \boldsymbol{\omega}^{r/g}\right) \tag{49}$$

Expanding the terms, Equation (37) becomes:

$$\mathbf{t}_r = \mathbf{J}_r\left(\frac{d\left(\boldsymbol{\omega}^{b/N}\right)}{dt}\right)^g + \mathbf{J}_r\left(\frac{d\left(\boldsymbol{\omega}^{g/b}\right)}{dt}\right)^g + \mathbf{J}_r\left(\frac{d\left(\boldsymbol{\omega}^{r/g}\right)}{dt}\right)^g$$

$$+ \left(\left(\boldsymbol{\omega}^{b/N} \times \mathbf{J}_r\boldsymbol{\omega}^{b/N}\right) + \left(\boldsymbol{\omega}^{g/b} \times \mathbf{J}_r\boldsymbol{\omega}^{b/N}\right)\right) \tag{50}$$

$$+ \left(\left(\boldsymbol{\omega}^{b/N} \times \mathbf{J}_r\boldsymbol{\omega}^{g/b}\right) + \left(\boldsymbol{\omega}^{g/b} \times \mathbf{J}_r\boldsymbol{\omega}^{g/b}\right)\right)$$

$$+ \left(\left(\boldsymbol{\omega}^{b/N} \times \mathbf{J}_r\boldsymbol{\omega}^{r/g}\right) + \left(\boldsymbol{\omega}^{g/b} \times \mathbf{J}_r\boldsymbol{\omega}^{r/g}\right)\right)$$

With the exception of the change in the inertia dyad, Rotor Terms 1, 2, 4, 5, 6, and 7 are identical to Gimbal Terms 1 through 6. By the same evaluation as shown in section III.D, Equations (51) through (56) follow.

1.   **Rotor Term 1**

$$\mathbf{J}_r\left(\frac{d\left(\boldsymbol{\omega}^{b/N}\right)}{dt}\right)^g = \begin{bmatrix} J_{r_1}\dot{\omega}_1 \\ J_{r_2}\dot{\omega}_2 \\ J_{r_3}\dot{\omega}_3 \end{bmatrix}\hat{b} + \begin{bmatrix} J_{r_1}\dot{\delta}\omega_{g_2} \\ -J_{r_2}\dot{\delta}\omega_{g_1} \\ 0 \end{bmatrix}\hat{g} \tag{51}$$

24

2. Rotor Term 2

$$\mathbf{J}_r\left(\frac{d\left(\boldsymbol{\omega}^{g/b}\right)}{dt}\right)^g = \begin{bmatrix} 0 \\ 0 \\ J_{r_3}\ddot{\delta} \end{bmatrix}\hat{g} \tag{52}$$

3. Rotor Term 4

$$\boldsymbol{\omega}^{b_g/N}\times\mathbf{J}_r\boldsymbol{\omega}^{b_g/N} = \begin{bmatrix} \omega_{2_g}\omega_{3_g}\left(J_{r_3}-J_{r_2}\right) \\ \omega_{1_g}\omega_{3_g}\left(J_{r_1}-J_{r_3}\right) \\ \omega_{1_g}\omega_{2_g}\left(J_{r_2}-J_{r_1}\right) \end{bmatrix}\hat{g} \tag{53}$$

4. Rotor Term 5

$$\boldsymbol{\omega}^{g/b}\times\mathbf{J}_r\boldsymbol{\omega}^{b/N} = \begin{bmatrix} -J_{r_2}\dot{\delta}\omega_{g_2} \\ J_{r_1}\dot{\delta}\omega_{g_1} \\ 0 \end{bmatrix}\hat{g} \tag{54}$$

5. Rotor Term 6

$$\boldsymbol{\omega}^{b/N}\times\mathbf{J}_g\boldsymbol{\omega}^{g/b} = \begin{bmatrix} J_{r_3}\dot{\delta}\omega_{g_2} \\ -J_{r_3}\dot{\delta}\omega_{g_1} \\ 0 \end{bmatrix}\hat{g} \tag{55}$$

6. Rotor Term 7

$$\boldsymbol{\omega}^{g/b}\times\mathbf{J}_g\boldsymbol{\omega}^{g/b} = 0 \tag{56}$$

Rotor Term 3, 8 and 9 will be evaluated in full.

7. Rotor Term 3

Again, $\mathbf{J}_r$ is removed from the derivative and because $\boldsymbol{\omega}^{r/g}$ is defined in the gimbal frame the result is simply:

$$\mathbf{J}_r \left(\frac{d\left(\mathbf{\omega}^{r/g} \right)}{dt} \right)^g = \begin{bmatrix} J_{r_1}\dot{\Omega} \\ 0 \\ 0 \end{bmatrix} \hat{g} \tag{57}$$

8.   Rotor Term 8

Using $\vec{\omega}^{b_g/N}$ in the gimbal frame and $\vec{\omega}^{r/g}$, the cross product becomes:

$$\mathbf{\omega}^{b/N} \times \mathbf{J}_r \mathbf{\omega}^{r/g} = \mathbf{\omega}^{b_g/N} \times \mathbf{J}_r \Omega \hat{g}_1$$

$$= \begin{bmatrix} \omega_{g_1} \\ \omega_{g_2} \\ \omega_{g_3} \end{bmatrix} \times \begin{bmatrix} J_{r_1}\Omega \\ 0 \\ 0 \end{bmatrix} \tag{58}$$

$$= \begin{bmatrix} 0 \\ J_{r_1}\Omega\omega_{g_3} \\ -J_{r_1}\Omega\omega_{g_2} \end{bmatrix} \hat{g}$$

9.   Rotor Term 9

Both $\mathbf{\omega}^{g/b}$ and $\mathbf{\omega}^{r/g}$ are defined in the gimbal frame so the cross product is:

$$\mathbf{\omega}^{g/b} \times \mathbf{J}_r \mathbf{\omega}^{r/g} = \dot{\delta}\hat{g}_3 \times \mathbf{J}_r \Omega \hat{g}_1$$

$$= \begin{bmatrix} 0 \\ 0 \\ \dot{\delta} \end{bmatrix} \times \begin{bmatrix} J_{r_1}\Omega \\ 0 \\ 0 \end{bmatrix} \tag{59}$$

$$= \begin{bmatrix} 0 \\ J_{r_1}\Omega\dot{\delta} \\ 0 \end{bmatrix} \hat{g}$$

Using the previously stated assumption that the rotor is symmetric about the $\hat{g}_1$ axis, we assume that J_{r_2} equals J_{r_3}, and the simplified equation becomes Equation (60)

.

$$t_r = \begin{bmatrix} J_{r_1}\dot{\omega}_1 \\ J_{r_2}\dot{\omega}_2 \\ J_{r_2}\dot{\omega}_3 \end{bmatrix}\hat{b} + \begin{bmatrix} J_{r_1}\dot{\delta}\omega_{g_2} \\ -J_{r_2}\dot{\delta}\omega_{g_1} \\ 0 \end{bmatrix}\hat{g} + \begin{bmatrix} 0 \\ 0 \\ J_{r_3}\ddot{\delta} \end{bmatrix}\hat{g} + \begin{bmatrix} J_{r_1}\dot{\Omega} \\ 0 \\ 0 \end{bmatrix}\hat{g}$$

$$+ \begin{bmatrix} 0 \\ \omega_{1_g}\omega_{3_g}\left(J_{r_1}-J_{r_2}\right) \\ \omega_{1_g}\omega_{2_g}\left(J_{r_2}-J_{r_1}\right) \end{bmatrix}\hat{g} + \begin{bmatrix} -J_{r_2}\dot{\delta}\omega_{g_2} \\ J_{r_1}\dot{\delta}\omega_{g_1} \\ 0 \end{bmatrix}\hat{g} + \begin{bmatrix} J_{r_3}\dot{\delta}\omega_{g_2} \\ -J_{r_3}\dot{\delta}\omega_{g_1} \\ 0 \end{bmatrix}\hat{g}$$

$$+ \begin{bmatrix} 0 \\ J_{r_1}\Omega\omega_{g_3} \\ -J_{r_1}\Omega\omega_{g_2} \end{bmatrix}\hat{g} + \begin{bmatrix} 0 \\ J_{r_1}\Omega\dot{\delta} \\ 0 \end{bmatrix}\hat{g} \tag{60}$$

F.   EQUATIONS OF MOTION FOR THE SYSTEM

Substituting Equations (34), (46) and (60) into Equation (24) the full equations of motion for a single CMG attached to a rigid body can be written as Equation (61).

$$t_{ext} = \begin{bmatrix} J_{b_1}\dot{\omega}_1 \\ J_{b_2}\dot{\omega}_2 \\ J_{b_3}\dot{\omega}_3 \end{bmatrix}\hat{b} + \begin{bmatrix} J_{g_1}\dot{\omega}_1 \\ J_{g_2}\dot{\omega}_2 \\ J_{g_3}\dot{\omega}_3 \end{bmatrix}\hat{b} + \begin{bmatrix} J_{r_1}\dot{\omega}_1 \\ J_{r_2}\dot{\omega}_2 \\ J_{r_2}\dot{\omega}_3 \end{bmatrix}\hat{b} + \begin{bmatrix} \left(J_{b_3}-J_{b_2}\right)\omega_2\omega_3 \\ \left(J_{b_1}-J_{b_3}\right)\omega_1\omega_3 \\ \left(J_{b_2}-J_{b_1}\right)\omega_1\omega_2 \end{bmatrix}\hat{b}$$

$$+ \begin{bmatrix} \left(J_{g_3}-J_{g_2}\right)\omega_{2_g}\omega_{3_g} \\ \left(J_{g_1}-J_{g_3}\right)\omega_{1_g}\omega_{3_g} \\ \left(J_{g_2}-J_{g_1}\right)\omega_{1_g}\omega_{2_g} \end{bmatrix}\hat{g} + \begin{bmatrix} 0 \\ \left(J_{r_1}-J_{r_2}\right)\omega_{1_g}\omega_{3_g} \\ \left(J_{r_2}-J_{r_1}\right)\omega_{1_g}\omega_{2_g} \end{bmatrix}\hat{g} + \begin{bmatrix} 0 \\ 0 \\ J_{g_3}\ddot{\delta} \end{bmatrix}\hat{g} + \begin{bmatrix} 0 \\ 0 \\ J_{r_3}\ddot{\delta} \end{bmatrix}\hat{g}$$

$$+ \begin{bmatrix} J_{g_1}\dot{\delta}\omega_{g_2} \\ -J_{g_2}\dot{\delta}\omega_{g_1} \\ 0 \end{bmatrix}\hat{g} + \begin{bmatrix} -J_{g_2}\dot{\delta}\omega_{g_2} \\ J_{g_1}\dot{\delta}\omega_{g_1} \\ 0 \end{bmatrix}\hat{g} + \begin{bmatrix} J_{g_3}\dot{\delta}\omega_{g_2} \\ -J_{g_3}\dot{\delta}\omega_{g_1} \\ 0 \end{bmatrix}\hat{g} + \begin{bmatrix} J_{r_1}\dot{\delta}\omega_{g_2} \\ -J_{r_2}\dot{\delta}\omega_{g_1} \\ 0 \end{bmatrix}\hat{g}$$

$$+ \begin{bmatrix} -J_{r_2}\dot{\delta}\omega_{g_2} \\ J_{r_1}\dot{\delta}\omega_{g_1} \\ 0 \end{bmatrix}\hat{g} + \begin{bmatrix} J_{r_3}\dot{\delta}\omega_{g_2} \\ -J_{r_3}\dot{\delta}\omega_{g_1} \\ 0 \end{bmatrix}\hat{g} + \begin{bmatrix} J_{r_1}\dot{\Omega} \\ 0 \\ 0 \end{bmatrix}\hat{g} + \begin{bmatrix} 0 \\ J_{r_1}\Omega\omega_{g_3} \\ -J_{r_1}\Omega\omega_{g_2} \end{bmatrix}\hat{g} + \begin{bmatrix} 0 \\ J_{r_1}\Omega\dot{\delta} \\ 0 \end{bmatrix}\hat{g} \tag{61}$$

In the original equation form, the reduced model referenced earlier in this document is shown in Equation (62).

$$\mathbf{t}_{CMG} = \left(J_{r_3} + J_{g_3} \right) \ddot{\delta} \hat{g}_1 + \left(\boldsymbol{\omega}^{b/N} \times \mathbf{h}_{CMG} \right) + \left(\boldsymbol{\omega}^{g/b} \times \mathbf{h}_{CMG} \right) \tag{62}$$

where $\mathbf{h}_{CMG} \equiv \mathbf{J}_r \boldsymbol{\omega}^{r/g}$. Based on Equation (61), the reduced model can also be written as Equation (63).

$$\mathbf{t}_{CMG} = \left[\begin{bmatrix} 0 \\ 0 \\ \left(J_{r_3} + J_{g_3} \right) \ddot{\delta} \end{bmatrix} + \begin{bmatrix} 0 \\ J_{r_1} \Omega \omega_{g_3} \\ -J_{r_1} \Omega \omega_{g_2} \end{bmatrix} + \begin{bmatrix} 0 \\ J_{r_1} \Omega \dot{\delta} \\ 0 \end{bmatrix} \right] \hat{g} \tag{63}$$

G.   HIGH FIDELITY SYSTEM DYNAMICS

We make the notational simplification that:

$$I_i \equiv J_{b_i} + J_{g_i} + J_{r_i} \tag{64}$$

Rearranging Equation (61) to solve for $\dot{\omega}$ we obtain

$$\begin{bmatrix} \dot{\omega}_1 \\ \dot{\omega}_2 \\ \dot{\omega}_3 \end{bmatrix} \hat{b} = \begin{bmatrix} \dfrac{1}{I_1} & 0 & 0 \\ 0 & \dfrac{1}{I_2} & 0 \\ 0 & 0 & \dfrac{1}{I_3} \end{bmatrix} \left[\begin{bmatrix} \left(J_{b_3} - J_{b_2} \right) \omega_2 \omega_3 \\ \left(J_{b_1} - J_{b_3} \right) \omega_1 \omega_3 \\ \left(J_{b_2} - J_{b_1} \right) \omega_1 \omega_2 \end{bmatrix} \hat{b} + \begin{bmatrix} \left(J_{g_3} - J_{g_2} \right) \omega_{2_g} \omega_{3_g} \\ \left(J_{g_1} - J_{g_3} \right) \omega_{1_g} \omega_{3_g} \\ \left(J_{g_2} - J_{g_1} \right) \omega_{1_g} \omega_{2_g} \end{bmatrix} \hat{g} \right.$$

$$+ \begin{bmatrix} 0 \\ \left(J_{r_1} - J_{r_2} \right) \omega_{1_g} \omega_{3_g} \\ \left(J_{r_2} - J_{r_1} \right) \omega_{1_g} \omega_{2_g} \end{bmatrix} \hat{g} + \begin{bmatrix} 0 \\ 0 \\ J_{g_3} \ddot{\delta} \end{bmatrix} \hat{g} + \begin{bmatrix} 0 \\ 0 \\ J_{r_3} \ddot{\delta} \end{bmatrix} \hat{g}$$

$$+ \begin{bmatrix} J_{g_1} \dot{\delta} \omega_{g_2} \\ -J_{g_2} \dot{\delta} \omega_{g_1} \\ 0 \end{bmatrix} \hat{g} + \begin{bmatrix} -J_{g_2} \dot{\delta} \omega_{g_2} \\ J_{g_1} \dot{\delta} \omega_{g_1} \\ 0 \end{bmatrix} \hat{g} + \begin{bmatrix} J_{g_3} \dot{\delta} \omega_{g_2} \\ -J_{g_3} \dot{\delta} \omega_{g_1} \\ 0 \end{bmatrix} \hat{g}$$

$$+ \begin{bmatrix} J_{r_1} \dot{\delta} \omega_{g_2} \\ -J_{r_2} \dot{\delta} \omega_{g_1} \\ 0 \end{bmatrix} \hat{g} + \begin{bmatrix} -J_{r_2} \dot{\delta} \omega_{g_2} \\ J_{r_1} \dot{\delta} \omega_{g_1} \\ 0 \end{bmatrix} \hat{g} + \begin{bmatrix} J_{r_3} \dot{\delta} \omega_{g_2} \\ -J_{r_3} \dot{\delta} \omega_{g_1} \\ 0 \end{bmatrix} \hat{g}$$

$$\left. + \begin{bmatrix} J_{r_1} \dot{\Omega} \\ 0 \\ 0 \end{bmatrix} \hat{g} + \begin{bmatrix} 0 \\ J_{r_1} \Omega \omega_{g_3} \\ -J_{r_1} \Omega \omega_{g_2} \end{bmatrix} \hat{g} + \begin{bmatrix} 0 \\ J_{r_1} \Omega \dot{\delta} \\ 0 \end{bmatrix} \hat{g} - \begin{bmatrix} T_{ext_1} \\ T_{ext_2} \\ T_{ext_3} \end{bmatrix} \hat{b} \right] \tag{65}$$

Clearly, this equation could be simplified; however, because the purpose of modeling is to determine the relative significance of the various terms, it will be left in its expanded form. This equation remains the effect of one CMG only. In order to increase the fidelity of the model and obtain results that are comparable to experimental data, it is necessary to expand the equations to an N-CMG constellation. A 4-CMG system is shown in Figure 6 as an example of a typical control system.
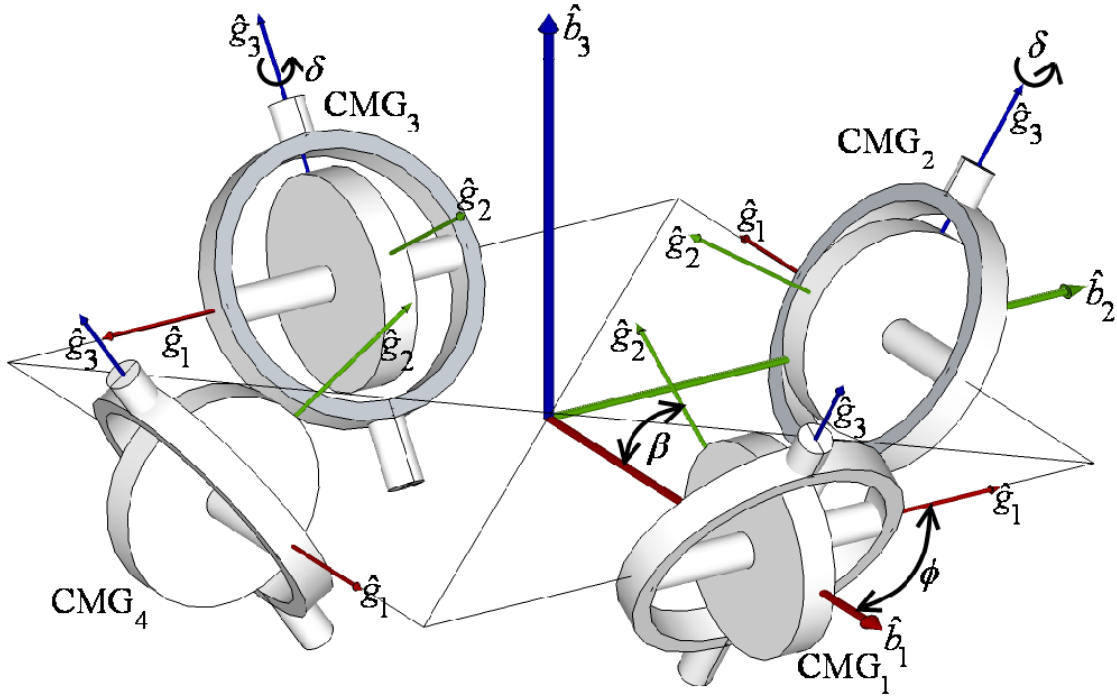
Figure 6. Four CMG pyramid configuration. Both ϕ (offset) and β (skew) angles are fixed, determined by the mounting of the CMGs with respect to the spacecraft reference frame ($\hat{b}_1, \hat{b}_2, \hat{b}_3$).

While the majority of the CMG terms have been left in the gimbal frame of reference, the transformation matrices are required both to convert the angular velocity of the body into the gimbal frame and to convert the gimbal torque into the body frame for integration.

Figure 6 shows that each CMG undergoes three rotations between the gimbal frame of reference and the body frame of reference. Initially each CMG axis is aligned with the body axis, therefore the first rotation is a rotation about the $\hat{g}_3$ axis to create an

29

offset angle between each CMG. In this model, CMG#1 rotates 90°, CMG#2 rotation 180°, CMG#3 rotates 270° and CMG#4 rotates 360°. Then each CMG is rotated about its spin axis ($\hat{g}_1$) an angle of β. This is the baseline position of each CMG. In order to create torque, each CMG then rotates an angle δ about its own $\hat{g}_3$ axis. The rotation matrices are therefore:

$$\mathbf{DCM}_{\hat{g}_3}(\phi) = \begin{bmatrix} \cos(\phi) & -\sin(\phi) & 0 \\ \sin(\phi) & \cos(\phi) & 0 \\ 0 & 0 & 1 \end{bmatrix}$$

$$\mathbf{DCM}_{\hat{g}_1}(\beta) = \begin{bmatrix} 1 & 0 & 0 \\ 0 & \cos(\beta) & -\sin(\beta) \\ 0 & \sin(\beta) & \cos(\beta) \end{bmatrix} \tag{66}$$

$$\mathbf{DCM}_{\hat{g}_3}(\delta) = \begin{bmatrix} \cos(\delta) & -\sin(\delta) & 0 \\ \sin(\delta) & \cos(\delta) & 0 \\ 0 & 0 & 1 \end{bmatrix}$$

The complete transformation matrix from the body frame to the gimbal frame is:

$$\mathbf{DCM}_{\hat{g}_3}(\delta) \cdot \mathbf{DCM}_{\hat{g}_1}(\beta) \cdot \mathbf{DCM}_{\hat{g}_3}(\phi) \tag{67}$$

Or

$$\mathbf{C}^{G/B} = \begin{bmatrix} c\delta c\phi\text{-}s\delta c\beta s\phi & c\delta s\phi\text{+}s\delta c\beta c\phi & s\delta s\beta \\ \text{-}s\delta c\phi\text{-}c\delta c\beta s\phi & \text{-}s\delta s\phi\text{+}c\delta c\beta c\phi & c\delta s\beta \\ s\beta s\phi & \text{-}s\beta c\phi & c\beta \end{bmatrix} \tag{68}$$

where $c\delta \equiv \cos(\delta), s\delta \equiv \sin(\delta), c\phi \equiv \cos(\phi), s\phi \equiv \sin(\phi), c\beta \equiv \cos(\beta)$, and $s\beta \equiv \sin(\beta)$. Using the relationship:

$$\left[\mathbf{C}^{B/A}\right]^{-1} = \left[\mathbf{C}^{B/A}\right]^{T} = \mathbf{C}^{A/B} \tag{69}$$

the DCM from the gimbal frame to the body frame is:

$$\mathbf{C}^{B/G} = \begin{bmatrix} c\delta c\phi\text{-}s\delta c\beta s\phi & \text{-}s\delta c\phi\text{-}c\delta c\beta s\phi & s\beta s\phi \\ c\delta s\phi\text{+}s\delta c\beta c\phi & \text{-}s\delta s\phi\text{+}c\delta c\beta c\phi & \text{-}s\beta c\phi \\ s\delta s\beta & c\delta s\beta & c\beta \end{bmatrix} \tag{70}$$

30

Section Notes

[27] Bong Wie, Space Vehicle Dynamics and Control, 2nd ed. (Reston, VA: American Institute of Aeronautics and Astronautics, 2008), 332, 403.

THIS PAGE INTENTIONALLY LEFT BLANK

IV. VERIFICATION OF MATHEMATICAL MODELS

A. SIMULINK MODEL

In order to verify the equations, a SIMULINK model was created, which evaluated the equations given control inputs of $\ddot{\delta}$. A function block was created that accepted as inputs the body quaternions (q) and angular velocities (ω) and the CMG input of $\ddot{\delta}$. The block was programmed to output both $\dot{q}$ and $\dot{\omega}$ as well as a variety of intermediate values for CMG torque contributions and angular momentums of the system. The function block accomplished the various frame of reference transformations and calculated each term of Equations (61) and (65) for further analysis. Shown in Figure 7, it was used to accomplish both open and closed loop simulations.
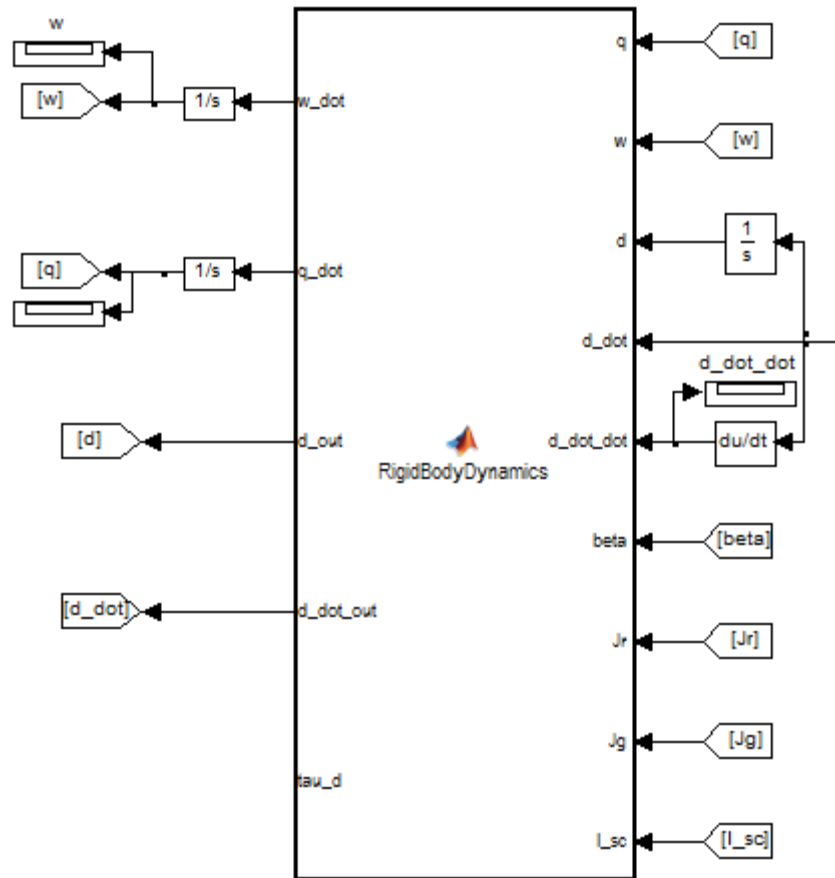

Figure 7.   System Dynamics function block.

The open loop simulations involved directly inputting values into the function block in order to calculate the CMG response.

The closed loop simulation used an Eigenaxis Rotational Maneuver controller to generate a required control torque in the body frame. The quaternion error was calculated using Equation (71)[28]

$$\mathbf{q}_e = \begin{bmatrix} q_c(4) & q_c(3) & -q_c(2) & -q_c(1) \\ -q_c(3) & q_c(4) & q_c(1) & -q_c(2) \\ q_c(2) & -q_c(1) & q_c(4) & -q_c(3) \\ q_c(1) & q_c(2) & q_c(3) & q_c(4) \end{bmatrix} \begin{bmatrix} q_1 \\ q_2 \\ q_3 \\ q_4 \end{bmatrix} \tag{71}$$

where q_c is the commanded quaternion vector and q is the body quaternion. The control torque was then generated using Equation (72).[29]

$$\mathbf{u} = -K_p \mathbf{I}_b \mathbf{q}_e \begin{bmatrix} 1 & 2 & 3 \end{bmatrix} - K_d \mathbf{I}_b \boldsymbol{\omega} + \boldsymbol{\omega} \times \mathbf{I}_b \boldsymbol{\omega} \tag{72}$$

K_p and K_d are the proportional and derivative gains, respectively, calculated using Equations (73) and (74) and $\mathbf{q}_e \begin{bmatrix} 1 & 2 & 3 \end{bmatrix}$ indicates that only the first three elements of $\mathbf{q}_e$ are used in the calculations.

$$K_p = \omega_n^2 \tag{73}$$

$$K_d = 2\omega_n \zeta \tag{74}$$

The control torque was then used to calculate the required gimbal angle, rate and acceleration. Gimbal rate was calculated using pseudo-inverse steering logic with null motion singularity avoidance.

From Equations (23) and (24), the external torque on the spacecraft can be written as

$$\mathbf{t}_{ext} = \left(\frac{d(\mathbf{H}_{tot})}{dt} \right)^N = \left(\frac{d(\mathbf{H}_{tot})}{dt} \right)^b + \boldsymbol{\omega}^{b/N} \times \mathbf{H}_{tot} \tag{75}$$

The total angular momentum from Equation (23) can be restated as

$$\mathbf{H}_{tot} = \mathbf{H}_b + \mathbf{h}_{CMG} = \mathbf{J}_b \boldsymbol{\omega}^{b/N} + \mathbf{h}_{CMG} \tag{76}$$

where $\mathbf{h}_{CMG} \equiv \mathbf{H}_g + \mathbf{H}_r$. Combining Equations (75) and (76) we obtain

$$t_{\text{ext}} = \left(\mathbf{J_b} \dot{\boldsymbol{\omega}}^{b/N} + \dot{\mathbf{h}}_{\text{CMG}} \right) + \left(\boldsymbol{\omega}^{b/N} \times \left(\mathbf{J_b} \boldsymbol{\omega}^{b/N} + \mathbf{h}_{\text{CMG}} \right) \right) \tag{77}$$

The control torque **u** is defined as the torque generated by the CMGs and is therefore

$$\mathbf{u} = -\left(\dot{\mathbf{h}}_{\text{CMG}} + \boldsymbol{\omega}^{b/N} \times \mathbf{h}_{\text{CMG}} \right) \tag{78}$$

For the purposes of developing an equation for gimbal rate, the angular momentum of the CMG system is simplified beyond even the reduced model. The complete angular momentum of the CMG is assumed to be

$$\mathbf{h}_{\text{CMG}} = J_{r_i} \Omega \hat{g}_1 \tag{79}$$

For a system of n-CMGs, and defining $h_0 = J_{r_i} \Omega$ the angular momentum of the CMGs in the body frame would be

$$\mathbf{h}_{\text{CMG}}\hat{b} = \sum_{i=1}^{n} h_0 \begin{bmatrix} c\delta_i c\phi_i - s\delta_i c\beta s\phi_i \\ c\delta_i s\phi_i + s\delta_i c\beta c\phi_i \\ s\delta_i s\beta \end{bmatrix} \tag{80}$$

The transformation vector is the first column of the DCM from the gimbal frame to the body frame ($\mathbf{C}^{B/G}$). Having defined the angular momentum of the CMG thus, the time derivative of the angular momentum vector is therefore

$$\dot{\mathbf{h}}_{\text{CMG}}\hat{b} = \sum_{i=1}^{n} h_0 \dot{\delta}_i \begin{bmatrix} -s\delta_i c\phi_i - c\delta_i c\beta s\phi_i \\ -s\delta_i s\phi_i + c\delta_i c\beta c\phi_i \\ c\delta_i s\beta \end{bmatrix} \tag{81}$$

where the transformation vector is the derivative of the first column of the DCM from the gimbal frame to the body frame. If we define

$$\mathbf{a_i} \equiv \begin{bmatrix} -s\delta_i c\phi_i - c\delta_i c\beta s\phi_i \\ -s\delta_i s\phi_i + c\delta_i c\beta c\phi_i \\ c\delta_i s\beta \end{bmatrix} \tag{82}$$

and

$$\mathbf{A} \equiv h_0 \left[\mathbf{a_1} \middle| \mathbf{a_2} \middle| \cdots \mathbf{a_n} \right] \tag{83}$$

Equation(81) becomes

35

$$\dot{\mathbf{h}} = \mathbf{A}\dot{\boldsymbol{\delta}} \tag{84}$$

Combining Equation(78) and (84) the gimbal rate can be obtained as

$$\dot{\boldsymbol{\delta}} = \mathbf{A}^{-1}\left(-\mathbf{u} - \boldsymbol{\omega}^{b/N} \times \mathbf{h}_{CMG}\right) \tag{85}$$

which was used in Section I as Equation (11). Equation (85) is only valid for $n = 3$, therefore a more general approach uses the pseudo-inverse shown in Equation (86).

$$\dot{\boldsymbol{\delta}} = \left(\mathbf{A}^T\left(\mathbf{A}\mathbf{A}^T\right)^{-1}\right)\left(-\mathbf{u} - \boldsymbol{\omega}^{b/N} \times \mathbf{h}_{CMG}\right) \tag{86}$$

A known issue with obtaining the gimbal rates using a pseudo-inverse technique such as Equation (86) is the existence of singular states. A singular state "occurs when all the individual CMG torque output vectors a_i are perpendicular to the commanded torque direction."[30] One technique to avoid singularities is to use null motion added to Equation (86) such that the gimbal rates becomes

$$\dot{\boldsymbol{\delta}} = \left(\mathbf{A}^T\left(\mathbf{A}\mathbf{A}^T + \lambda\mathbf{I}\right)^{-1}\right)\left(-\mathbf{u} - \boldsymbol{\omega}^{b/N} \times \mathbf{h}_{CMG}\right) \tag{87}$$

where the value for λ is controlled by the singularity measure. The singularity measure is calculated using Equation (88).

$$m = \sqrt{\det\left(AA^T\right)} \tag{88}$$

The value for λ is calculated as shown in Equation (89).

$$\begin{aligned}
&\text{if } m \geq 0.5 \\
&\quad \lambda = 0 \\
&\text{if } m < 0.5 \\
&\quad \lambda = 10
\end{aligned} \tag{89}$$

The commanded gimbal rate was then used to calculate commanded gimbal angle and acceleration for use in the simulation.

B.   OPEN LOOP SIMULATIONS

Several open loop Monte Carlo simulations were conducted where random values were generated for $\ddot{\boldsymbol{\delta}}$, $\boldsymbol{\omega}$, Ω, $\mathbf{J}_r$, and $\mathbf{J}_g$. The values were bounded as shown in Table 1.

36

	Maximum Value	Minimum Value
$\ddot{\delta}$	10 rad/sec^2	-10 rad/sec^2
ω	0.5 rad/sec (-28.5 °/sec)	-0.5 rad/sec (-28.5 °/sec)
Ω	1000 rpm	15,000 rpm
J_r	$HW_{rotor\ scaling} \begin{bmatrix} 1.25 & 0 & 0 \\ 0 & 0.625 & 0 \\ 0 & 0 & 0.625 \end{bmatrix} kg \cdot m^2$	$HW_{rotor\ scaling} \begin{bmatrix} 0.75 & 0 & 0 \\ 0 & 0.375 & 0 \\ 0 & 0 & 0.375 \end{bmatrix} kg \cdot m^2$
J_g	$HW_{gimbal\ scaling} \begin{bmatrix} 1.25 & 0 & 0 \\ 0 & 1.25 & 0 \\ 0 & 0 & 1.25 \end{bmatrix} kg \cdot m^2$	$HW_{gimbal\ scaling} \begin{bmatrix} 0.75 & 0 & 0 \\ 0 & 0.75 & 0 \\ 0 & 0 & 0.75 \end{bmatrix}$ $kg \cdot m^2$

Table 1.   Bounds for initial open loop Monte Carlo simulation.

Baseline moment of inertia tensors were chosen to simulate a representative CMG table and a CubeSat,. The system level moment of inertia tensor remained constant while the remainder of the inputs were bounded as shown in Table 1. Inertia tensor values for the CMG gimbal and rotor were obtained from Honeywell. Due to the proprietary nature of the information, the actual values are not used; however normalized representative values are used. The values of the CMG inertia tensors were varied by 25%. Because $\ddot{\delta}$ is the control variable the bounds were set well outside the typical values (10 rad/sec^2 equates to 576 deg/sec^2). Ω values were estimated using an industry value for the lower bound and proposed industry values for the upper. The simulation was run for one million steps and the output values for the CMG gimbal and output torques were calculated at each step.

A measure of how accurate the reduced model was compared to the full model was computed using the values for the CMG Axis 2 (output) and Axis 3 (gimbal) torque at each step. The accuracy for each data point was calculated using the standard relative error, shown in Equation (90).

$$\text{measure of accuracy} = \frac{\left\|T_{full} - T_{red}\right\|_2}{\left\|T_{full}\right\|_2} \tag{90}$$

The reduced model has no terms that contribute to Axis 1. Therefore, the measure of accuracy calculation could not be completed for that accuracy. However, in order to confirm that it is correct for the reduced model to disregard Axis 1, a measure of significance was conducted where the magnitude of the Axis 1 torque was compared to the magnitude of the Axis 2 (output) torque, shown in Equation (91).

$$\text{measure of signifigance} = \frac{\left\|T_{full}\left(\text{Axis 1}\right)\right\|_2}{\left\|T_{full}\left(\text{Axis 2}\right)\right\|_2} \tag{91}$$

The accuracy of the entire model was then estimated by taking the infinity-norm of the vectors generated by Equations (90) and (91). The infinity norm of the vector is the maximum value so the measure of accuracy in Table 2 represents the worst case scenario of the reduced model.

System	Axis 1 Measure of Significance	Axis 2 Measure of Accuracy	Axis 3 Measure of Accuracy
CubeSat	0.0138	0.00208	0.01195
CMG Table	0.0141	0.00854	0.01365

Table 2.   Open loop measure of accuracy.

Table 2 shows that Axis 1 torque is less than 1% of the Axis 2 (output) torque, meaning that the reduced model failure to include any magnitude for that Axis is appropriate for most models. It also shows that the reduced model is accurate to within 1% for all input values. A more detailed representation of the accuracy of the model is shown in Figure 8, which shows the histograms of the error vectors for the CMG table.
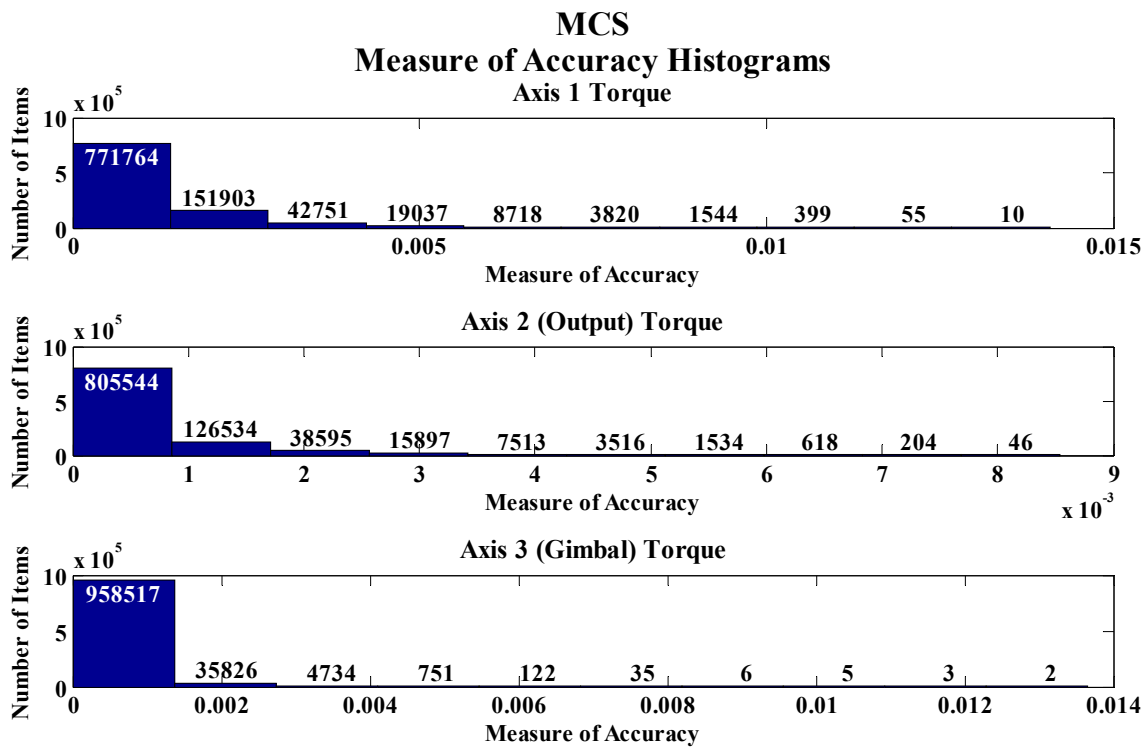
Figure 8.   Histogram of open loop simulations for the CMG table. Note that while there are outliers, the model is generally accurate to 0.00137 for the input torque and 0.00086 for the output or an order of magnitude better than the worst outliers.

Figure 9 shows the histogram data for the CubeSat simulations revealing similar results.

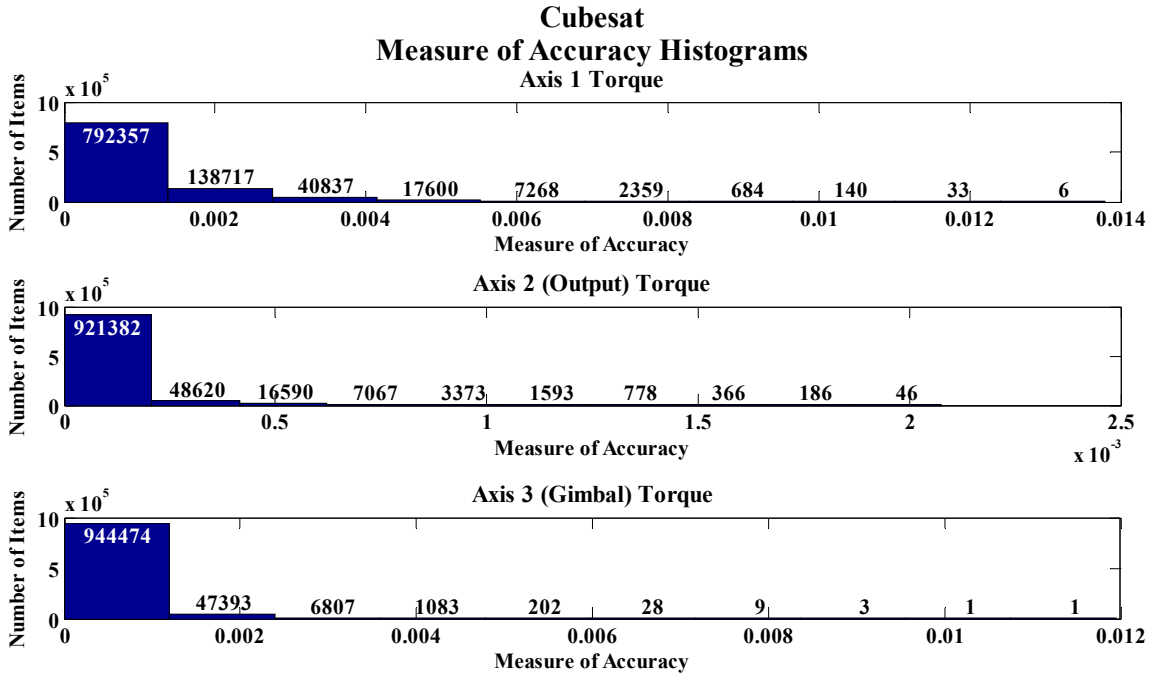**Cubesat**
Measure of Accuracy Histograms

Figure 9.   Histogram of open loop simulations for the CubeSat values. Again, while outliers are present, the model is generally accurate an order of magnitude better than the worst outliers.

C.   CLOSED LOOP SIMULATIONS

A closed loop Monte Carlo simulation was run where the initial Euler Angles were varied from 0-180 and the Rotor and Gimbal Inertia Tensors were allowed to vary by 25%, similar to the Open Loop Monte Carlo but with Ω values were held constant and the angular velocity and gimbal acceleration determined by the simulation. In each simulation the commanded end state was zero pitch, roll and yaw and zero angular velocity. During each simulation, the value of each of the six Gimbal and nine Rotor terms were calculated for each axis of each CMG. As shown in Figure 10 each term's magnitude was calculated in each CMG axis.

For each CMG:

$$\begin{bmatrix} a_1 \\ b_1 \\ c_1 \end{bmatrix}_{G1} \begin{bmatrix} a_2 \\ b_2 \\ c_2 \end{bmatrix}_{G2} \cdots \begin{bmatrix} a_6 \\ b_6 \\ c_6 \end{bmatrix}_{G6} \begin{bmatrix} a_7 \\ b_7 \\ c_7 \end{bmatrix}_{R1} \cdots \begin{bmatrix} a_{15} \\ b_{15} \\ c_{15} \end{bmatrix}_{R9}$$

Figure 10.   Value of each of the terms contributing to the overall CMG torque.

At every time step, the magnitude of each of the terms was divided by the term with the maximum value to determine the relative magnitude of each term as shown in Figure 11.

$$\begin{bmatrix} \dfrac{|a_1|}{Max[a_1 \cdots a_{15}]} & \dfrac{|a_2|}{Max[a_1 \cdots a_{15}]} & \cdots & \dfrac{|a_{14}|}{Max[a_1 \cdots a_{15}]} & \dfrac{|a_{15}|}{Max[a_1 \cdots a_{15}]} \end{bmatrix}$$

Figure 11.   Relative magnitude calculation conducted at each time step.

For each complete simulation, the maximum relative magnitudes were saved for comparison. The Monte Carlo simulation was run for 10,000 iterations. The saved data was analyzed to determine if there were any conditions in which the terms that are not included in the reduced model, i.e., those terms believed to be small enough to be ignored, are significant. The maximum values for the Monte Carlo for the Gimbal terms and Rotor terms for Axis 1 torque are in Table 3, Axis 2 (output) are in Table 4, and Axis 3 (gimbal) torque are in Table 5.

Gimbal Term 1	Gimbal Term 2	Gimbal Term 3	Gimbal Term 4	Gimbal Term 5
$\mathbf{J}_g\left(\dfrac{d\left(\boldsymbol{\omega}^{b/N}\right)}{dt}\right)^g$	$\mathbf{J}_g\left(\dfrac{d\left(\boldsymbol{\omega}^{g/b}\right)}{dt}\right)^g$ Reduced Model	$\boldsymbol{\omega}^{b_g/N}\times\mathbf{J}_g\boldsymbol{\omega}^{b_g/N}$	$\boldsymbol{\omega}^{g/b}\times\mathbf{J}_g\boldsymbol{\omega}^{b/N}$	$\boldsymbol{\omega}^{b/N}\times\mathbf{J}_g\boldsymbol{\omega}^{g/b}$
100.00%	0.0000%	100.00%	100.00%	100.00%
Gimbal Term 6	Rotor Term 1	Rotor Term 2	Rotor Term 3	Rotor Term 4
$\boldsymbol{\omega}^{g/b}\times\mathbf{J}_g\boldsymbol{\omega}^{g/b}$	$\mathbf{J}_r\left(\dfrac{d\left(\boldsymbol{\omega}^{b/N}\right)}{dt}\right)^g$	$\mathbf{J}_r\left(\dfrac{d\left(\boldsymbol{\omega}^{g/b}\right)}{dt}\right)^g$ Reduced Model	$\mathbf{J}_r\left(\dfrac{d\left(\boldsymbol{\omega}^{r/g}\right)}{dt}\right)^g$	$\boldsymbol{\omega}^{b_g/N}\times\mathbf{J}_r\boldsymbol{\omega}^{b_g/N}$
0.0000%	100.00%	0.0000%	0.0000%	100.00%
Rotor Term 5	Rotor Term 6	Rotor Term 7	Rotor Term 8	Rotor Term 9
$\boldsymbol{\omega}^{g/b}\times\mathbf{J}_r\boldsymbol{\omega}^{b/N}$	$\boldsymbol{\omega}^{b/N}\times\mathbf{J}_g\boldsymbol{\omega}^{g/b}$	$\boldsymbol{\omega}^{g/b}\times\mathbf{J}_g\boldsymbol{\omega}^{g/b}$	$\boldsymbol{\omega}^{b/N}\times\mathbf{J}_r\boldsymbol{\omega}^{r/g}$ Reduced Model	$\boldsymbol{\omega}^{g/b}\times\mathbf{J}_r\boldsymbol{\omega}^{r/g}$ Reduced Model
58.418%	62.481%	0.0000%	0.0000%	0.0000%

Table 3.　Maximum relative values for Gimbal and Rotor terms in Axis 1.

Gimbal Term 1	Gimbal Term 2	Gimbal Term 3	Gimbal Term 4	Gimbal Term 5
$\mathbf{J}_g\left(\dfrac{d\left(\boldsymbol{\omega}^{b/N}\right)}{dt}\right)^g$	$\mathbf{J}_g\left(\dfrac{d\left(\boldsymbol{\omega}^{g/b}\right)}{dt}\right)^g$ Reduced Model	$\boldsymbol{\omega}^{b_g/N}\times\mathbf{J}_g\boldsymbol{\omega}^{b_g/N}$	$\boldsymbol{\omega}^{g/b}\times\mathbf{J}_g\boldsymbol{\omega}^{b/N}$	$\boldsymbol{\omega}^{b/N}\times\mathbf{J}_g\boldsymbol{\omega}^{g/b}$
1.0527%	0.0000%	0.27903%	1.0197%	1.0374%
Gimbal Term 6	Rotor Term 1	Rotor Term 2	Rotor Term 3	Rotor Term 4
$\boldsymbol{\omega}^{g/b}\times\mathbf{J}_g\boldsymbol{\omega}^{g/b}$	$\mathbf{J}_r\left(\dfrac{d\left(\boldsymbol{\omega}^{b/N}\right)}{dt}\right)^g$	$\mathbf{J}_r\left(\dfrac{d\left(\boldsymbol{\omega}^{g/b}\right)}{dt}\right)^g$ Reduced Model	$\mathbf{J}_r\left(\dfrac{d\left(\boldsymbol{\omega}^{r/g}\right)}{dt}\right)^g$	$\boldsymbol{\omega}^{b_g/N}\times\mathbf{J}_r\boldsymbol{\omega}^{b_g/N}$
0.0000%	0.29326%	0.0000%	0.0000%	0.27903%
Rotor Term 5	Rotor Term 6	Rotor Term 7	Rotor Term 8	Rotor Term 9
$\boldsymbol{\omega}^{g/b}\times\mathbf{J}_r\boldsymbol{\omega}^{b/N}$	$\boldsymbol{\omega}^{b/N}\times\mathbf{J}_g\boldsymbol{\omega}^{g/b}$	$\boldsymbol{\omega}^{g/b}\times\mathbf{J}_g\boldsymbol{\omega}^{g/b}$	$\boldsymbol{\omega}^{b/N}\times\mathbf{J}_r\boldsymbol{\omega}^{r/g}$ Reduced Model	$\boldsymbol{\omega}^{g/b}\times\mathbf{J}_r\boldsymbol{\omega}^{r/g}$ Reduced Model
0.57009%	0.30515%	0.0000%	100.00%	100.00%

Table 4.   Maximum relative values for Gimbal and Rotor terms in Axis 2.

Gimbal Term 1	Gimbal Term 2	Gimbal Term 3	Gimbal Term 4	Gimbal Term 5
$\mathbf{J}_g \left(\dfrac{d\left(\boldsymbol{\omega}^{b/N}\right)}{dt} \right)^g$	$\mathbf{J}_g \left(\dfrac{d\left(\boldsymbol{\omega}^{g/b}\right)}{dt} \right)^g$ Reduced Model	$\boldsymbol{\omega}^{b_g/N} \times \mathbf{J}_g \boldsymbol{\omega}^{b_g/N}$	$\boldsymbol{\omega}^{g/b} \times \mathbf{J}_g \boldsymbol{\omega}^{b/N}$	$\boldsymbol{\omega}^{b/N} \times \mathbf{J}_g \boldsymbol{\omega}^{g/b}$
0.0000%	100.00%	0.32274%	0.0000%	0.0000%
Gimbal Term 6	Rotor Term 1	Rotor Term 2	Rotor Term 3	Rotor Term 4
$\boldsymbol{\omega}^{g/b} \times \mathbf{J}_g \boldsymbol{\omega}^{g/b}$	$\mathbf{J}_r \left(\dfrac{d\left(\boldsymbol{\omega}^{b/N}\right)}{dt} \right)^g$	$\mathbf{J}_r \left(\dfrac{d\left(\boldsymbol{\omega}^{g/b}\right)}{dt} \right)^g$ Reduced Model	$\mathbf{J}_r \left(\dfrac{d\left(\boldsymbol{\omega}^{r/g}\right)}{dt} \right)^g$	$\boldsymbol{\omega}^{b_g/N} \times \mathbf{J}_r \boldsymbol{\omega}^{b_g/N}$
0.0000%	0.0000%	63.145%	0.0000%	0.30415%
Rotor Term 5	Rotor Term 6	Rotor Term 7	Rotor Term 8	Rotor Term 9
$\boldsymbol{\omega}^{g/b} \times \mathbf{J}_r \boldsymbol{\omega}^{b/N}$	$\boldsymbol{\omega}^{b/N} \times \mathbf{J}_g \boldsymbol{\omega}^{g/b}$	$\boldsymbol{\omega}^{g/b} \times \mathbf{J}_g \boldsymbol{\omega}^{g/b}$	$\boldsymbol{\omega}^{b/N} \times \mathbf{J}_r \boldsymbol{\omega}^{r/g}$ Reduced Model	$\boldsymbol{\omega}^{g/b} \times \mathbf{J}_r \boldsymbol{\omega}^{r/g}$ Reduced Model
0.0000%	0.0000%	0.0000%	100.00%	0.0000%

Table 5.   Maximum relative values for Gimbal and Rotor terms in Axis 3.

From this information we can see that Axis 1 shows the most amount of variation on which terms contribute most. However, the open loop analysis showed that the relative magnitude of the Axis 1 torque compared to the Axis 2 torque makes the overall output negligible. Recall that the reduced model assumes that the Axis 1 torque is zero. For Axis 3, the terms that are not included in the reduced model do not exceed 0.3% at any point in the simulation. However, for Axis 2, several terms reach 1% significance and the accumulation of those terms could potentially reach 3%. This likely remains below the threshold of significance for most applications but could potentially be meaningful.

Section Notes

28 Bong Wie, Space Vehicle Dynamics and Control, 2nd ed. (Reston, VA: American Institute of Aeronautics and Astronautics, 2008), 403.

29 Ibid., 406.

30 Ibid., 440.

THIS PAGE INTENTIONALLY LEFT BLANK

V. EXPERIMENTAL VERIFICATION

A. HONEYWELL MOMENTUM CONTROL SYSTEM

In August 2011, a series of experimental maneuvers was conducted on Honeywell Space System's spacecraft attitude dynamics testbed. The testbed, shown in Figure 12, is capable of high-agility slewing, incorporating six 225 ft-lb CMGs.[31]

Figure 12.   Honeywell's Momentum Control System (MCS) testbed.

The testbed is capable of unlimited movement about the z-axis, and $\pm30°$ in the x and y-axes.[32] The vehicle has no umbilical to ground, using a wireless link for command and telemetry.[33] The air bearing has a 3200 pound load capacity and is mounted on a concrete base that is isolated from the surrounding building.[34] For the NPS experimental runs, the CMG rotor speed was set to 1000 rpm. The natural frequency of the testbed, used to calculate gains, was 0.4 Hz while the damping ratio was set to 0.7.

B. TRAPEZOID EXPERIMENTAL SETUP

Based on input from industry a standard trapezoid maneuver was created. The maneuver consists of a feedforward body angular velocity and quaternion paths. The process for calculated an industry maneuvers begins with establishing a desired set of Euler Angles. The example maneuver used was from $+2.25°$ pitch, $-20.25°$ roll and $0°$ yaw to $-2.25°$ pitch, $+20.25°$ roll and $0°$ yaw. The desired Euler Angles along with the maximum body angular velocity and maximum body acceleration are used to generate angular velocity paths that resemble trapezoids, as shown in Figure 13.
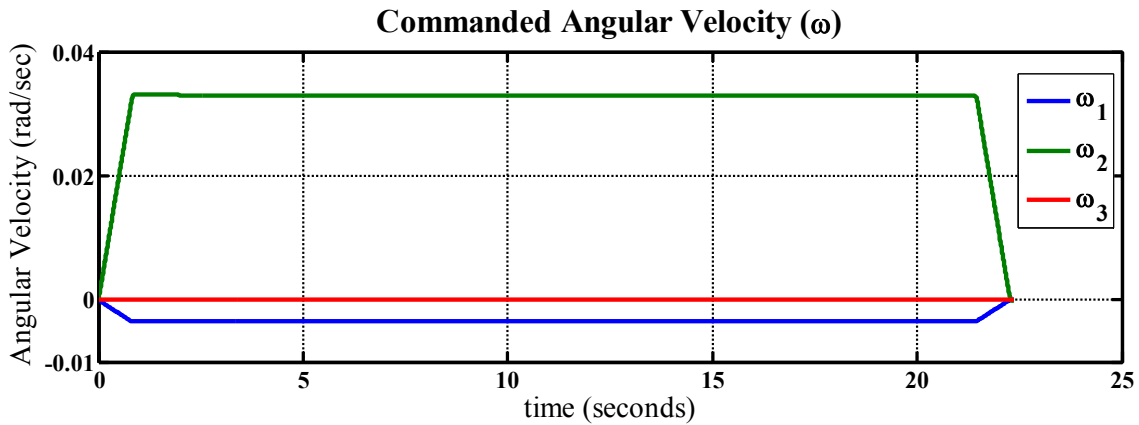

Figure 13.   Example of an industry standard trapezoid style maneuver.

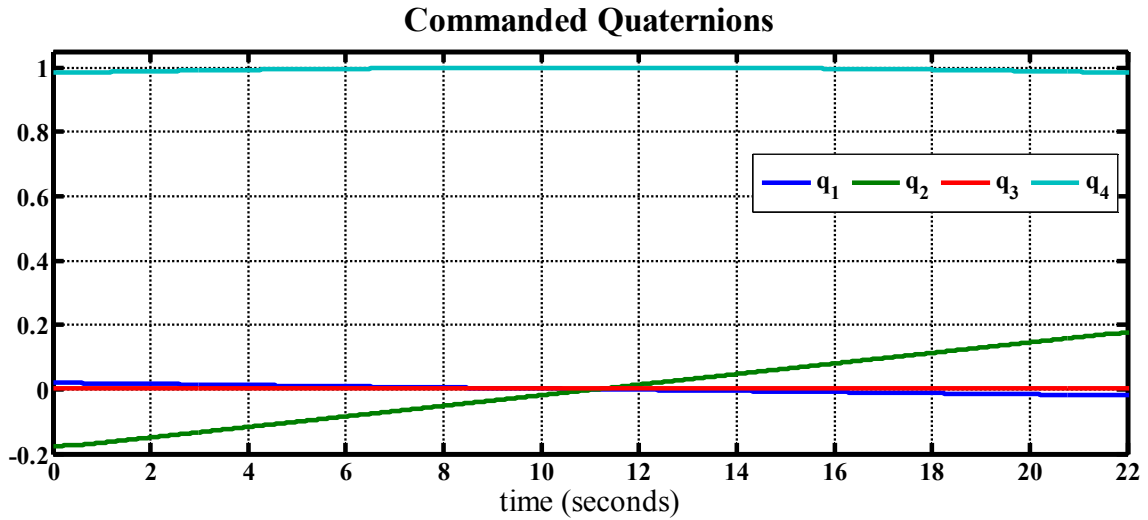The Commanded Euler Angles were also used to generate Commanded Quaternion paths, as shown in Figure 14.

Figure 14.   Commanded quaternions for an industry standard maneuver.

C.   COMPARISON OF RESULTS

The results of the simulation were compared in several ways. The simulation results were compared to the commanded angular velocity and quaternions to determine how well the simulation tracked the feedforward commands as shown in Figure 15 and Figure 16.
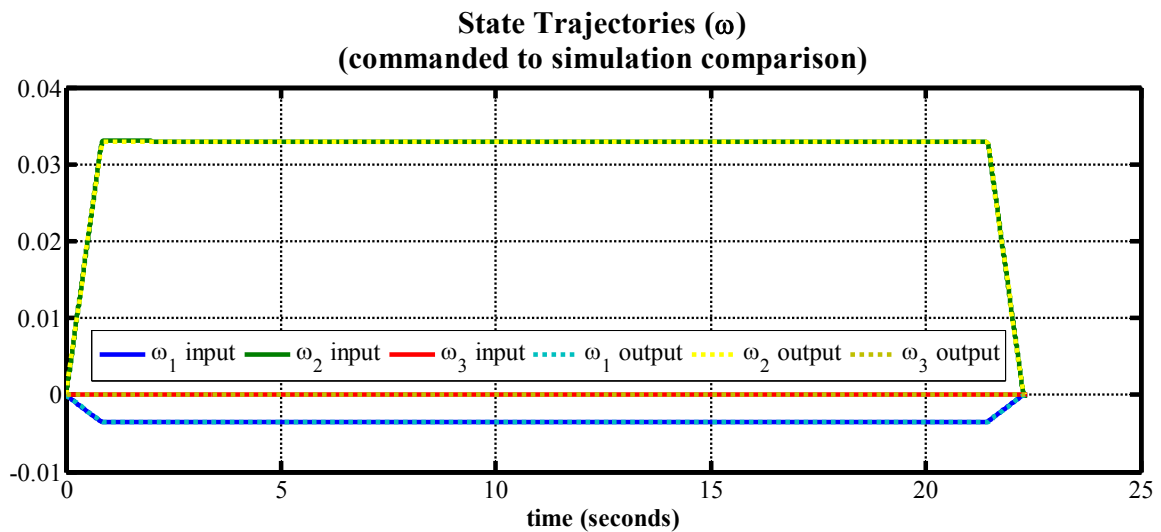

Figure 15.   Comparison of commanded angular velocity to simulation output angular velocity.

State Trajectories (q)
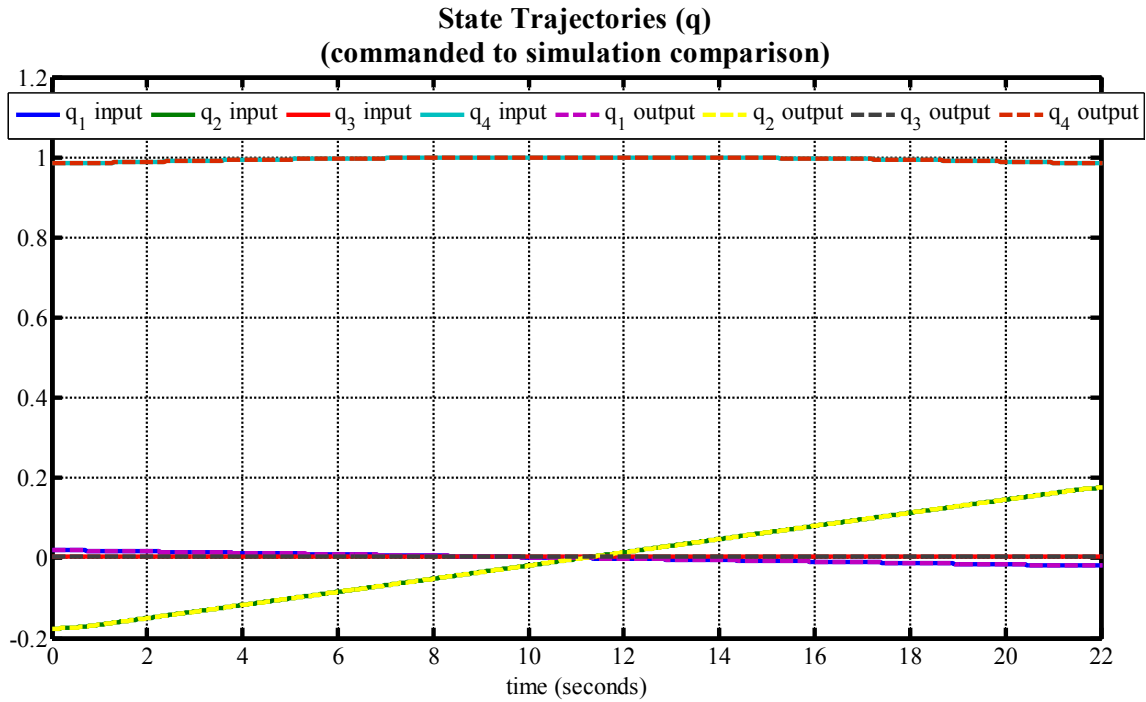**(commanded to simulation comparison)**

Figure 16.   Comparison of commanded quaternions to simulation output quaternions.

These figures show that the simulation tracks the input extremely well. This was confirmed by calculating the Root Mean Square(RMS) error of the commanded input versus the output.   The RMS error for the angular velocity is 1.9268×10^{-5} and 5.3755×10^{-6} for the quaternions.

The simulation results were also compared to the Honeywell MCS output of the same commanded angular velocity and quaternions to determine how well the simulation reflects the hardware as shown in Figure 17 and Figure 18.
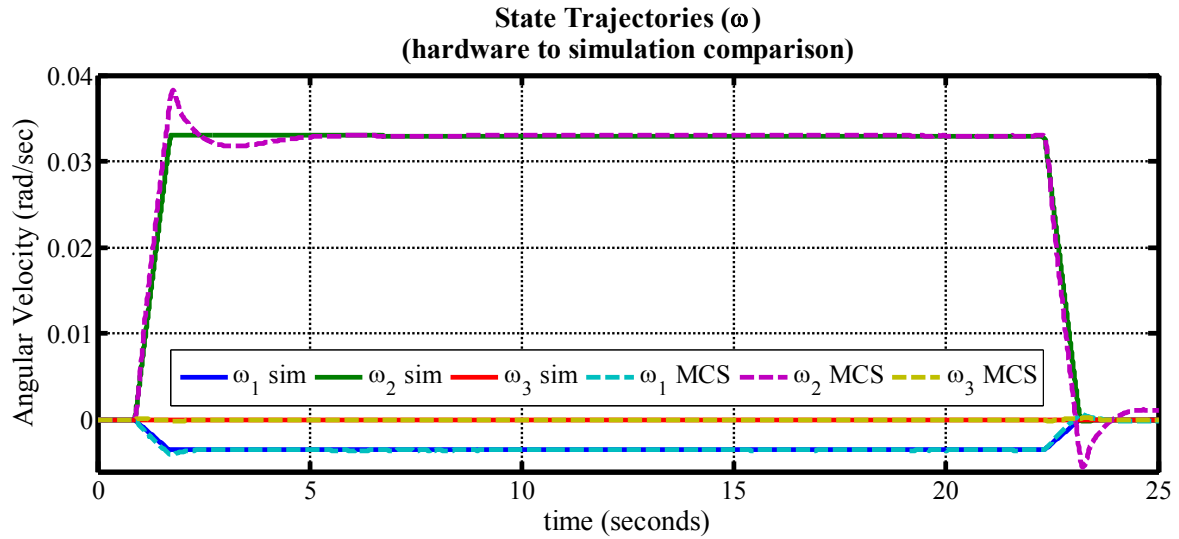
State Trajectories (ω)
(hardware to simulation comparison)

Figure 17.　　Comparison of simulation output angular velocity to
hardware output angular velocity.

State Trajectories (q)
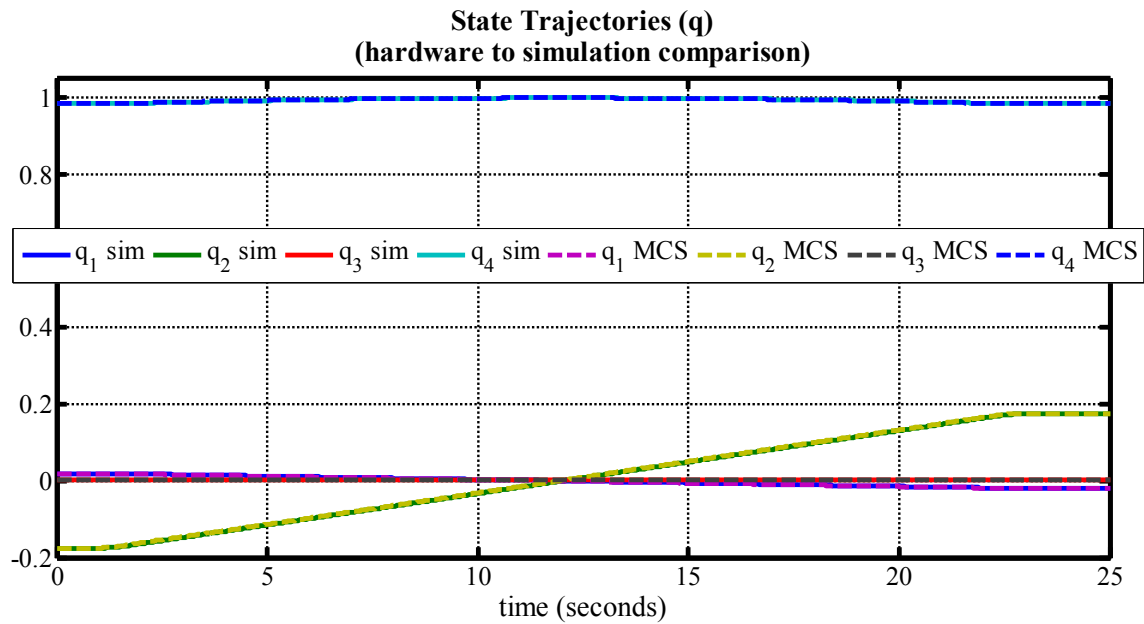**(hardware to simulation comparison)**

Figure 18.　　Comparison of simulation output quaternions to
hardware output quaternions.

Figure 17 shows that the physical hardware has transient responses not revealed by the simulation. These reflect inaccuracies in the transient response of the simulation. For instance; the simulation does not currently account for friction effects on the individual

51

CMG gimbals. Even with this transient error, the overall RMS error remains low. The RMS error for the angular velocity is 5.6897×10^{-4}; for the quaternions it is 9.0234×10^{-4}.

The Honeywell MCS data includes most of the information needed to calculate the values of the individual terms. The gimbal acceleration is not captured directly but gimbal torque is measured. Since all the other terms can be calculated, we can use the gimbal torque to solve for Gimbal Term 2 and Rotor Term 2. The maximum relative magnitudes of each term were calculated over the course of the simulation in the same manner as described in the closed loop analysis. Table 6 contains the maximum relative values for Axis 1. While this axis shows the most variation, the total magnitude of the torque in this axis remains small in relation to the Axis 2 or output torque.

Gimbal Term 1	Gimbal Term 2	Gimbal Term 3	Gimbal Term 4	Gimbal Term 5
$\mathbf{J}_g \left(\dfrac{d\left(\boldsymbol{\omega}^{b/N}\right)}{dt} \right)^g$	$\mathbf{J}_g \left(\dfrac{d\left(\boldsymbol{\omega}^{g/b}\right)}{dt} \right)^g$ Reduced Model	$\boldsymbol{\omega}^{b_g/N} \times \mathbf{J}_g \boldsymbol{\omega}^{b_g/N}$	$\boldsymbol{\omega}^{g/b} \times \mathbf{J}_g \boldsymbol{\omega}^{b/N}$	$\boldsymbol{\omega}^{b/N} \times \mathbf{J}_g \boldsymbol{\omega}^{g/b}$
90.5840%	0.0000%	100.0000%	72.6682%	100.0000%
Gimbal Term 6	Rotor Term 1	Rotor Term 2	Rotor Term 3	Rotor Term 4
$\boldsymbol{\omega}^{g/b} \times \mathbf{J}_g \boldsymbol{\omega}^{g/b}$	$\mathbf{J}_r \left(\dfrac{d\left(\boldsymbol{\omega}^{b/N}\right)}{dt} \right)^g$	$\mathbf{J}_r \left(\dfrac{d\left(\boldsymbol{\omega}^{g/b}\right)}{dt} \right)^g$ Reduced Model	$\mathbf{J}_r \left(\dfrac{d\left(\boldsymbol{\omega}^{r/g}\right)}{dt} \right)^g$	$\boldsymbol{\omega}^{b_g/N} \times \mathbf{J}_r \boldsymbol{\omega}^{b_g/N}$
0.0000%	54.2066%	0.0000%	0.0000%	100.0000%
Rotor Term 5	Rotor Term 6	Rotor Term 7	Rotor Term 8	Rotor Term 9
$\boldsymbol{\omega}^{g/b} \times \mathbf{J}_r \boldsymbol{\omega}^{b/N}$	$\boldsymbol{\omega}^{b/N} \times \mathbf{J}_g \boldsymbol{\omega}^{g/b}$	$\boldsymbol{\omega}^{g/b} \times \mathbf{J}_g \boldsymbol{\omega}^{g/b}$	$\boldsymbol{\omega}^{b/N} \times \mathbf{J}_r \boldsymbol{\omega}^{r/g}$ Reduced Model	$\boldsymbol{\omega}^{g/b} \times \mathbf{J}_r \boldsymbol{\omega}^{r/g}$ Reduced Model
36.0455%	27.2439%	0.0000%	0.0000%	0.0000%

Table 6. Maximum relative values for Gimbal and Rotor terms in Axis 1.

Table 7 shows the results for Axis 2. As expected the terms not included in the reduced model are negligible.

Gimbal Term 1	Gimbal Term 2	Gimbal Term 3	Gimbal Term 4	Gimbal Term 5
$\mathbf{J}_g\left(\dfrac{d\left(\boldsymbol{\omega}^{b/N}\right)}{dt}\right)^g$	$\mathbf{J}_g\left(\dfrac{d\left(\boldsymbol{\omega}^{g/b}\right)}{dt}\right)^g$ Reduced Model	$\boldsymbol{\omega}^{b_g/N}\times\mathbf{J}_g\boldsymbol{\omega}^{b_g/N}$	$\boldsymbol{\omega}^{g/b}\times\mathbf{J}_g\boldsymbol{\omega}^{b/N}$	$\boldsymbol{\omega}^{b/N}\times\mathbf{J}_g\boldsymbol{\omega}^{g/b}$
0.0059%	0.0000%	0.0000%	0.0059%	0.0059%

Gimbal Term 6	Rotor Term 1	Rotor Term 2	Rotor Term 3	Rotor Term 4
$\boldsymbol{\omega}^{g/b}\times\mathbf{J}_g\boldsymbol{\omega}^{g/b}$	$\mathbf{J}_r\left(\dfrac{d\left(\boldsymbol{\omega}^{b/N}\right)}{dt}\right)^g$	$\mathbf{J}_r\left(\dfrac{d\left(\boldsymbol{\omega}^{g/b}\right)}{dt}\right)^g$ Reduced Model	$\mathbf{J}_r\left(\dfrac{d\left(\boldsymbol{\omega}^{r/g}\right)}{dt}\right)^g$	$\boldsymbol{\omega}^{b_g/N}\times\mathbf{J}_r\boldsymbol{\omega}^{b_g/N}$
0.0000%	0.0017%	0.0000%	0.0000%	0.0017%

Rotor Term 5	Rotor Term 6	Rotor Term 7	Rotor Term 8	Rotor Term 9
$\boldsymbol{\omega}^{g/b}\times\mathbf{J}_r\boldsymbol{\omega}^{b/N}$	$\boldsymbol{\omega}^{b/N}\times\mathbf{J}_g\boldsymbol{\omega}^{g/b}$	$\boldsymbol{\omega}^{g/b}\times\mathbf{J}_g\boldsymbol{\omega}^{g/b}$	$\boldsymbol{\omega}^{b/N}\times\mathbf{J}_r\boldsymbol{\omega}^{r/g}$ Reduced Model	$\boldsymbol{\omega}^{g/b}\times\mathbf{J}_r\boldsymbol{\omega}^{r/g}$ Reduced Model
0.0034%	0.0017%	0.0000%	100.0000%	100.0000%

Table 7.   Maximum relative values for Gimbal and Rotor terms in Axis 2.

Table 8 shows the results for Axis 3. Again, the terms not included in the reduced model are negligible.

Gimbal Term 1	Gimbal Term 2	Gimbal Term 3	Gimbal Term 4	Gimbal Term 5
$\mathbf{J}_g\left(\dfrac{d\left(\boldsymbol{\omega}^{b/N}\right)}{dt}\right)^g$	$\mathbf{J}_g\left(\dfrac{d\left(\boldsymbol{\omega}^{g/b}\right)}{dt}\right)^g$ Reduced Model	$\boldsymbol{\omega}^{b_g/N}\times\mathbf{J}_g\boldsymbol{\omega}^{b_g/N}$	$\boldsymbol{\omega}^{g/b}\times\mathbf{J}_g\boldsymbol{\omega}^{b/N}$	$\boldsymbol{\omega}^{b/N}\times\mathbf{J}_g\boldsymbol{\omega}^{g/b}$
0.0000%	100.0000%	0.0000%	0.0000%	0.0000%
Gimbal Term 6	Rotor Term 1	Rotor Term 2	Rotor Term 3	Rotor Term 4
$\boldsymbol{\omega}^{g/b}\times\mathbf{J}_g\boldsymbol{\omega}^{g/b}$	$\mathbf{J}_r\left(\dfrac{d\left(\boldsymbol{\omega}^{b/N}\right)}{dt}\right)^g$	$\mathbf{J}_r\left(\dfrac{d\left(\boldsymbol{\omega}^{g/b}\right)}{dt}\right)^g$ Reduced Model	$\mathbf{J}_r\left(\dfrac{d\left(\boldsymbol{\omega}^{r/g}\right)}{dt}\right)^g$	$\boldsymbol{\omega}^{b_g/N}\times\mathbf{J}_r\boldsymbol{\omega}^{b_g/N}$
0.0000%	0.0000%	38.0356%	0.0000%	0.0017%
Rotor Term 5	Rotor Term 6	Rotor Term 7	Rotor Term 8	Rotor Term 9
$\boldsymbol{\omega}^{g/b}\times\mathbf{J}_r\boldsymbol{\omega}^{b/N}$	$\boldsymbol{\omega}^{b/N}\times\mathbf{J}_g\boldsymbol{\omega}^{g/b}$	$\boldsymbol{\omega}^{g/b}\times\mathbf{J}_g\boldsymbol{\omega}^{g/b}$	$\boldsymbol{\omega}^{b/N}\times\mathbf{J}_r\boldsymbol{\omega}^{r/g}$ Reduced Model	$\boldsymbol{\omega}^{g/b}\times\mathbf{J}_r\boldsymbol{\omega}^{r/g}$ Reduced Model
0.0000%	0.0000%	0.0000%	100.0000%	0.0000%

Table 8.   Maximum relative values for Gimbal and Rotor terms in Axis 3.

D.   OPTIMAL MANEUVER EXPERIMENTAL SETUP

In addition to the industry standard maneuver, the same initial and end Euler Angles were used to develop a time optimal maneuver. The time optimal maneuver commanded angular velocity is shown in Figure 19 and the commanded Quaternions are shown in Figure 20.
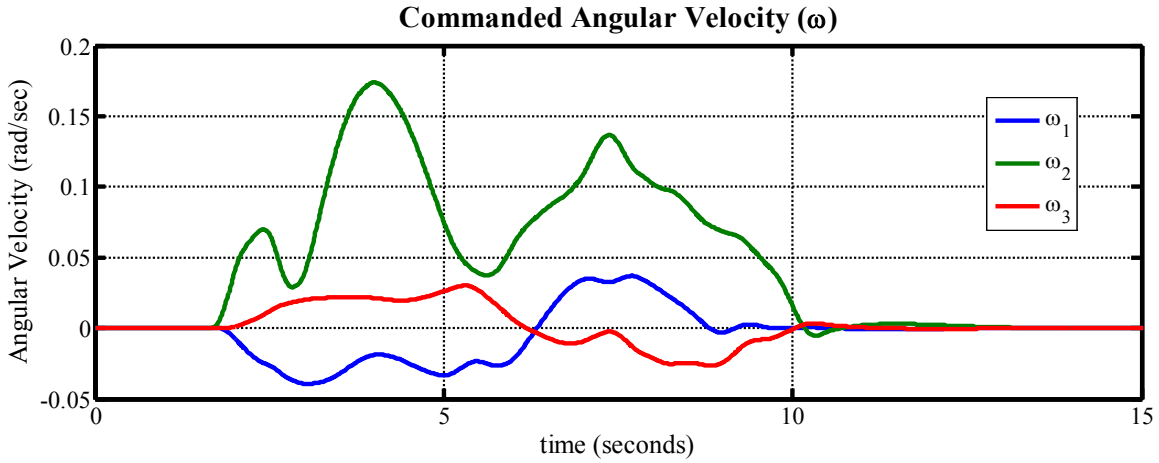
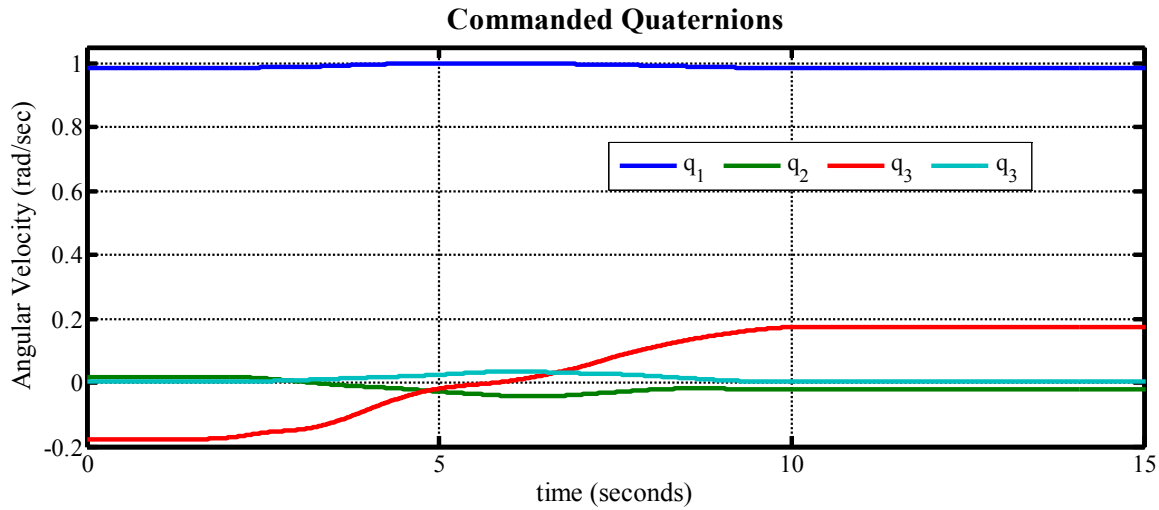Figure 19.   Time optimal commanded angular velocity.

Figure 20.   Time optimal commanded quaternions.

E.   COMPARISON OF RESULTS

The results of the simulation were compared in the same manner as the trapezoid maneuver. The simulation results were compared to the commanded angular velocity and quaternions to determine how well the simulation tracked the feedforward commands as shown in Figure 21 and Figure 22.
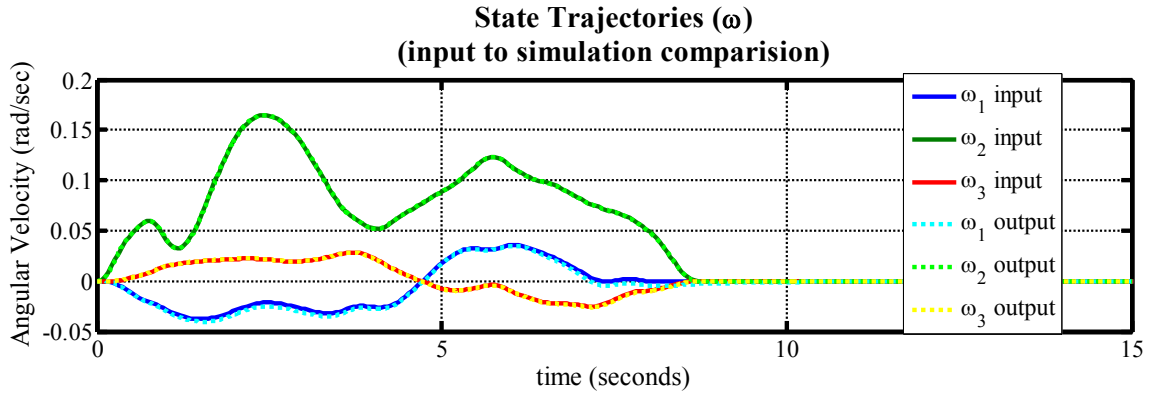
Figure 21.   Comparison of commanded angular velocity to simulation output angular velocity.
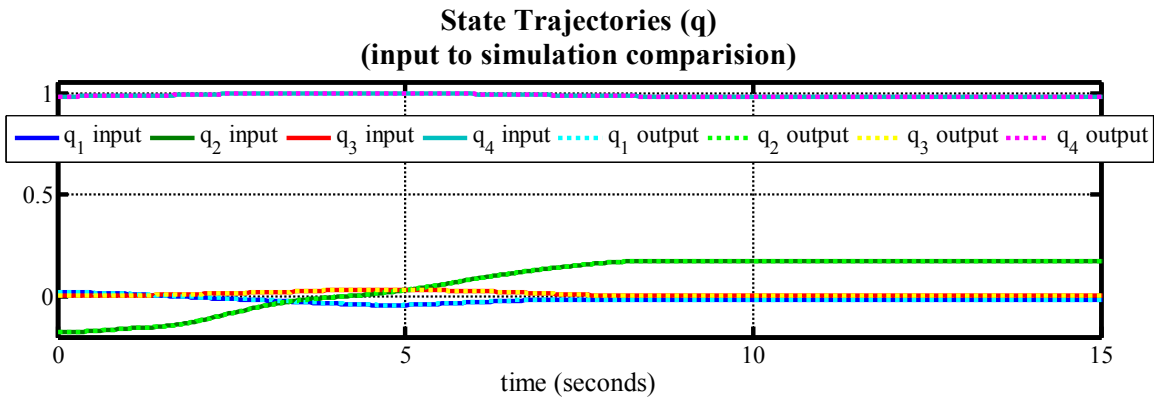

Figure 22.   Comparison of commanded quaternions to simulation output quaternions.

These figures show differences between the simulation input and output are negligible. This was again confirmed by calculating the RMS error of the commanded input versus the output. The RMS error for the angular velocity is 1.3003×10^{-3} and 6.5517×10^{-4} for the quaternions.

The simulation results were also compared to the Honeywell MCS output of the same commanded angular velocity and quaternions to determine how well the simulation reflects the hardware as shown in Figure 23 and Figure 24.
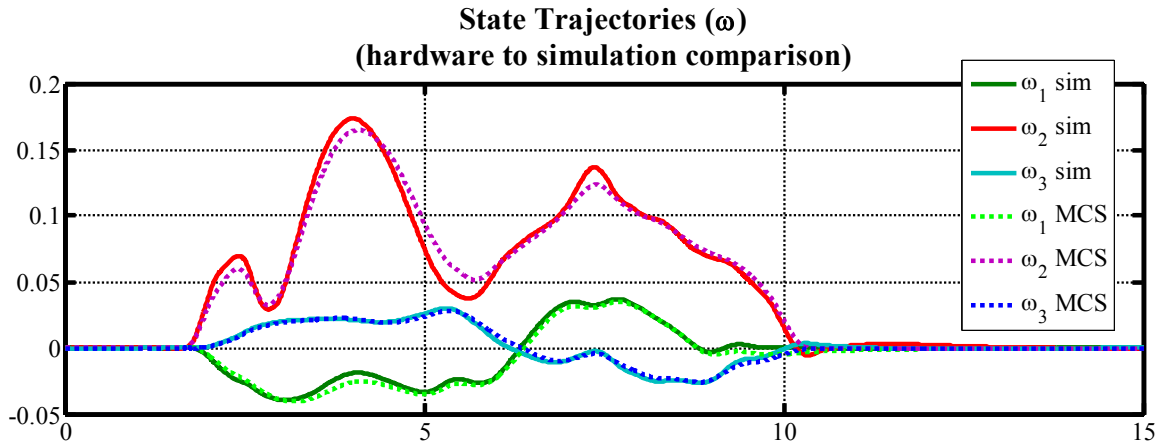
State Trajectories (ω)
(hardware to simulation comparison)

Figure 23.   Comparison of simulation output angular velocity to hardware output angular velocity.

State Trajectories (q)
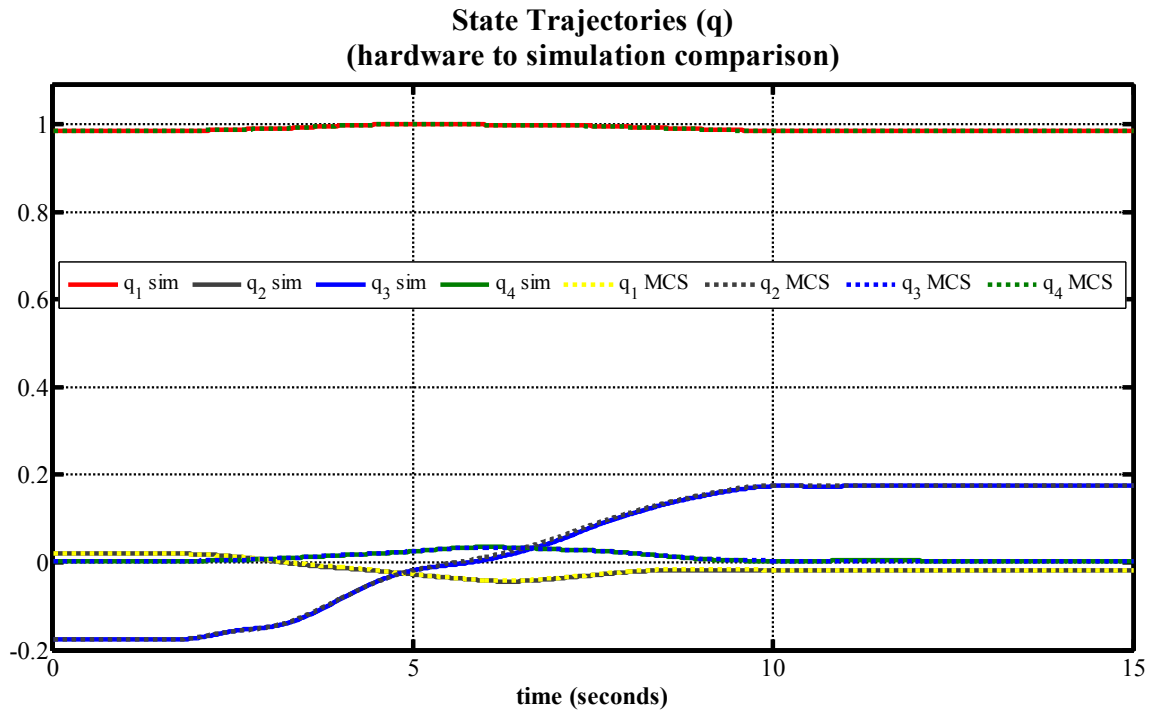**(hardware to simulation comparison)**

Figure 24.   Comparison of simulation output quaternions to hardware output quaternions.

Figure 23Figure 23.   again shows transient responses in the hardware not revealed by the simulation. The transient differences are greater in the optimal control maneuver than in the trapezoid maneuver due to the increased aggressiveness of the optimal control path.

57

This is also reflected in increased RMS error. The RMS error for the angular velocity is 3.5693×10^{-3} and 1.9205×10^{-3} for the quaternions.

The maximum relative magnitudes of each term were calculated over the course of the simulation in the same manner as the trapezoid maneuver. Table 9, Table 10, and Table 11 contain the maximum relative values for Axis 1, 2 and 3, respectively. The computed values are consistent with the expected results and with the trapezoid maneuver.

Gimbal Term 1	Gimbal Term 2	Gimbal Term 3	Gimbal Term 4	Gimbal Term 5
$\mathbf{J}_g\left(\dfrac{d\left(\boldsymbol{\omega}^{b/N}\right)}{dt}\right)^g$	$\mathbf{J}_g\left(\dfrac{d\left(\boldsymbol{\omega}^{g/b}\right)}{dt}\right)^g$ Reduced Model	$\boldsymbol{\omega}^{b_g/N}\times\mathbf{J}_g\boldsymbol{\omega}^{b_g/N}$	$\boldsymbol{\omega}^{g/b}\times\mathbf{J}_g\boldsymbol{\omega}^{b/N}$	$\boldsymbol{\omega}^{b/N}\times\mathbf{J}_g\boldsymbol{\omega}^{g/b}$
100.0000%	0.0000%	0.0000%	100.0000%	100.0000%
Gimbal Term 6	Rotor Term 1	Rotor Term 2	Rotor Term 3	Rotor Term 4
$\boldsymbol{\omega}^{g/b}\times\mathbf{J}_g\boldsymbol{\omega}^{g/b}$	$\mathbf{J}_r\left(\dfrac{d\left(\boldsymbol{\omega}^{b/N}\right)}{dt}\right)^g$	$\mathbf{J}_r\left(\dfrac{d\left(\boldsymbol{\omega}^{g/b}\right)}{dt}\right)^g$ Reduced Model	$\mathbf{J}_r\left(\dfrac{d\left(\boldsymbol{\omega}^{r/g}\right)}{dt}\right)^g$	$\boldsymbol{\omega}^{b_g/N}\times\mathbf{J}_r\boldsymbol{\omega}^{b_g/N}$
0.0000%	76.0712%	0.0000%	0.0000%	0.0000%
Rotor Term 5	Rotor Term 6	Rotor Term 7	Rotor Term 8	Rotor Term 9
$\boldsymbol{\omega}^{g/b}\times\mathbf{J}_r\boldsymbol{\omega}^{b/N}$	$\boldsymbol{\omega}^{b/N}\times\mathbf{J}_g\boldsymbol{\omega}^{g/b}$	$\boldsymbol{\omega}^{g/b}\times\mathbf{J}_g\boldsymbol{\omega}^{g/b}$	$\boldsymbol{\omega}^{b/N}\times\mathbf{J}_r\boldsymbol{\omega}^{r/g}$ Reduced Model	$\boldsymbol{\omega}^{g/b}\times\mathbf{J}_r\boldsymbol{\omega}^{r/g}$ Reduced Model
38.0356%	38.0356%	0.0000%	0.0000%	0.0000%

Table 9.   Maximum relative values for Gimbal and Rotor terms in Axis 1.

Gimbal Term 1	Gimbal Term 2	Gimbal Term 3	Gimbal Term 4	Gimbal Term 5
$\mathbf{J}_g\left(\dfrac{d\left(\boldsymbol{\omega}^{b/N}\right)}{dt}\right)^g$	$\mathbf{J}_g\left(\dfrac{d\left(\boldsymbol{\omega}^{g/b}\right)}{dt}\right)^g$ Reduced Model	$\boldsymbol{\omega}^{b_g/N}\times\mathbf{J}_g\boldsymbol{\omega}^{b_g/N}$	$\boldsymbol{\omega}^{g/b}\times\mathbf{J}_g\boldsymbol{\omega}^{b/N}$	$\boldsymbol{\omega}^{b/N}\times\mathbf{J}_g\boldsymbol{\omega}^{g/b}$
0.0280%	0.0000%	0.0000%	0.0280%	0.0280%
Gimbal Term 6	Rotor Term 1	Rotor Term 2	Rotor Term 3	Rotor Term 4
$\boldsymbol{\omega}^{g/b}\times\mathbf{J}_g\boldsymbol{\omega}^{g/b}$	$\mathbf{J}_r\left(\dfrac{d\left(\boldsymbol{\omega}^{b/N}\right)}{dt}\right)^g$	$\mathbf{J}_r\left(\dfrac{d\left(\boldsymbol{\omega}^{g/b}\right)}{dt}\right)^g$ Reduced Model	$\mathbf{J}_r\left(\dfrac{d\left(\boldsymbol{\omega}^{r/g}\right)}{dt}\right)^g$	$\boldsymbol{\omega}^{b_g/N}\times\mathbf{J}_r\boldsymbol{\omega}^{b_g/N}$
0.0000%	0.0081%	0.0000%	0.0000%	0.0068%
Rotor Term 5	Rotor Term 6	Rotor Term 7	Rotor Term 8	Rotor Term 9
$\boldsymbol{\omega}^{g/b}\times\mathbf{J}_r\boldsymbol{\omega}^{b/N}$	$\boldsymbol{\omega}^{b/N}\times\mathbf{J}_g\boldsymbol{\omega}^{g/b}$	$\boldsymbol{\omega}^{g/b}\times\mathbf{J}_g\boldsymbol{\omega}^{g/b}$	$\boldsymbol{\omega}^{b/N}\times\mathbf{J}_r\boldsymbol{\omega}^{r/g}$ Reduced Model	$\boldsymbol{\omega}^{g/b}\times\mathbf{J}_r\boldsymbol{\omega}^{r/g}$ Reduced Model
0.0162%	0.0081%	0.0000%	100.0000%	100.0000%

Table 10.   Maximum relative values for Gimbal and Rotor terms in Axis 2.

Gimbal Term 1	Gimbal Term 2	Gimbal Term 3	Gimbal Term 4	Gimbal Term 5
$\mathbf{J}_g\left(\dfrac{d\left(\boldsymbol{\omega}^{b/N}\right)}{dt}\right)^g$	$\mathbf{J}_g\left(\dfrac{d\left(\boldsymbol{\omega}^{g/b}\right)}{dt}\right)^g$ Reduced Model	$\boldsymbol{\omega}^{b_g/N}\times\mathbf{J}_g\boldsymbol{\omega}^{b_g/N}$	$\boldsymbol{\omega}^{g/b}\times\mathbf{J}_g\boldsymbol{\omega}^{b/N}$	$\boldsymbol{\omega}^{b/N}\times\mathbf{J}_g\boldsymbol{\omega}^{g/b}$
0.0000%	100.0000%	0.0000%	0.0000%	0.0000%
Gimbal Term 6	**Rotor Term 1**	**Rotor Term 2**	**Rotor Term 3**	**Rotor Term 4**
$\boldsymbol{\omega}^{g/b}\times\mathbf{J}_g\boldsymbol{\omega}^{g/b}$	$\mathbf{J}_r\left(\dfrac{d\left(\boldsymbol{\omega}^{b/N}\right)}{dt}\right)^g$	$\mathbf{J}_r\left(\dfrac{d\left(\boldsymbol{\omega}^{g/b}\right)}{dt}\right)^g$ Reduced Model	$\mathbf{J}_r\left(\dfrac{d\left(\boldsymbol{\omega}^{r/g}\right)}{dt}\right)^g$	$\boldsymbol{\omega}^{b_g/N}\times\mathbf{J}_r\boldsymbol{\omega}^{b_g/N}$
0.0000%	0.0000%	38.0356%	0.0000%	0.0081%
Rotor Term 5	**Rotor Term 6**	**Rotor Term 7**	**Rotor Term 8**	**Rotor Term 9**
$\boldsymbol{\omega}^{g/b}\times\mathbf{J}_r\boldsymbol{\omega}^{b/N}$	$\boldsymbol{\omega}^{b/N}\times\mathbf{J}_g\boldsymbol{\omega}^{g/b}$	$\boldsymbol{\omega}^{g/b}\times\mathbf{J}_g\boldsymbol{\omega}^{g/b}$	$\boldsymbol{\omega}^{b/N}\times\mathbf{J}_r\boldsymbol{\omega}^{r/g}$ Reduced Model	$\boldsymbol{\omega}^{g/b}\times\mathbf{J}_r\boldsymbol{\omega}^{r/g}$ Reduced Model
0.0000%	0.0000%	0.0000%	100.0000%	0.0000%

Table 11.   Maximum relative values for Gimbal and Rotor terms in Axis 3.

F.   NPS SATELLITE SIMULATOR TEST BED (STB)

The NPS Satellite Simulator Test Bed (STB) shown in Figure 25 is an Andrews Space Satellite Simulator tailored for use at NPS. Four seven ft-lb CMGs are mounted in a roof-down configuration on an attitude platform, which is supported by a spherical air bearing.
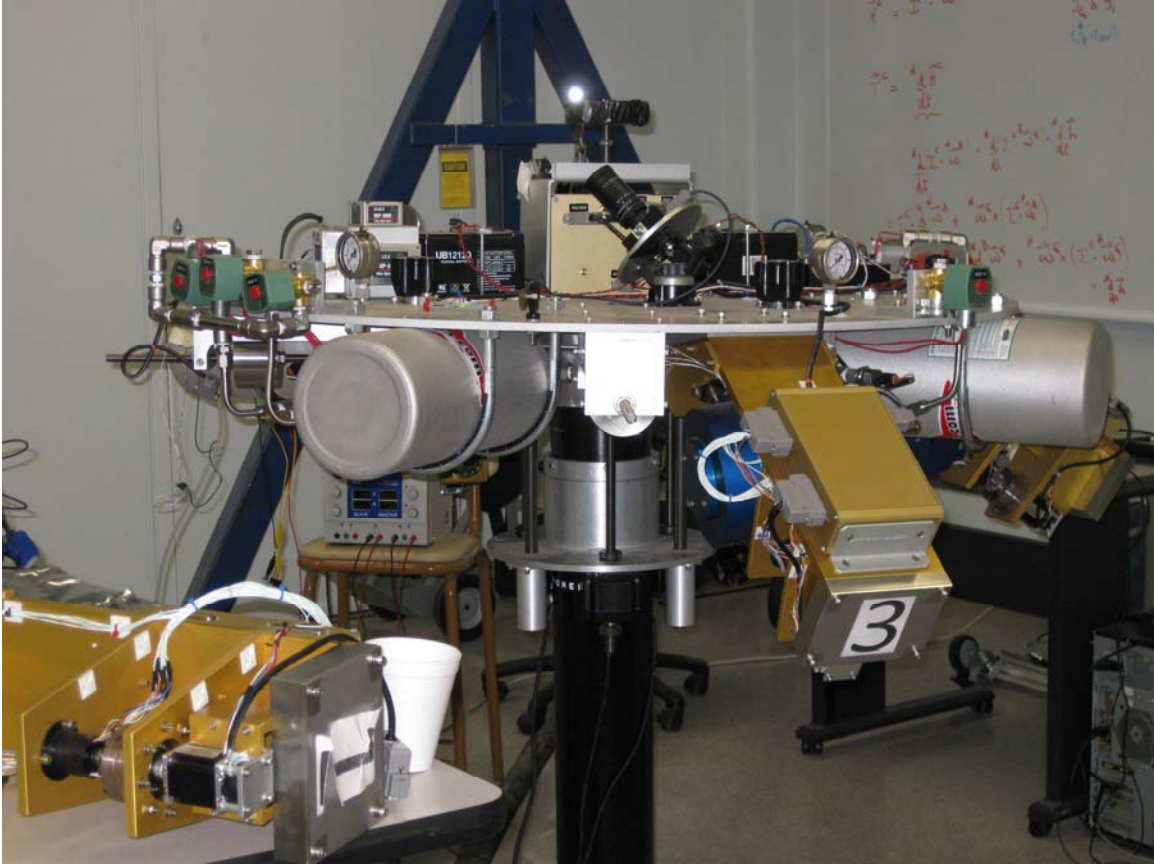
Figure 25.   NPS Satellite Simulator Test Bed (STB).

The simulator is capable of unlimited movement about the z-axis, and $\pm 45°$ in the x and y-axes. The rotor speed was set to 5000 rpm for the experimental maneuver.

G.   DESCRIPTIONS OF COMPARISON MANEUVER

Currently the STB is commanded using feedforward quaternions only. Additionally, CMG1 has malfunctioned and has been shut down, leaving only three functional CMGs. The test maneuver commanded quaternions are shown in Figure 26.

Commanded Quaternions
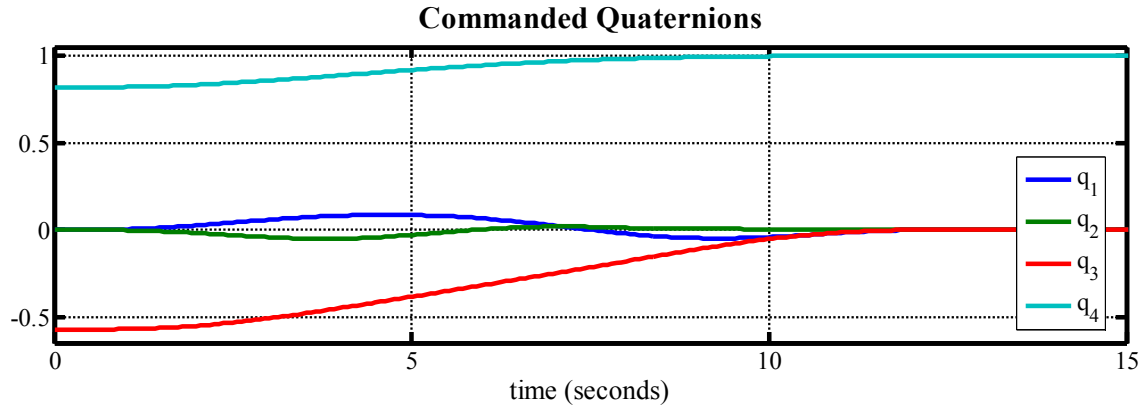
Figure 26.   STB commanded quaternions.

H.   COMPARISON OF RESULTS

Again, the results of the simulation were compared in several ways. The simulation results were compared to the commanded quaternions to determine how well the simulation tracked the feedforward commands as shown in Figure 27.

State Trajectories (q)
(input to simulation comparision)

Figure 27.   Comparison of commanded quaternions to simulation output quaternions.

Figure 27 shows that the simulation exhibits a slight delay before tracking the commanded quaternions. The delay may be caused by a lack of expected feedforward angular velocity. This also leads to an increased RMS error for this data of 1.1970×10^{-2}.

The simulation results were also compared to the STB output of the same commanded quaternions to determine how well the simulation reflects the hardware as shown in Figure 28.
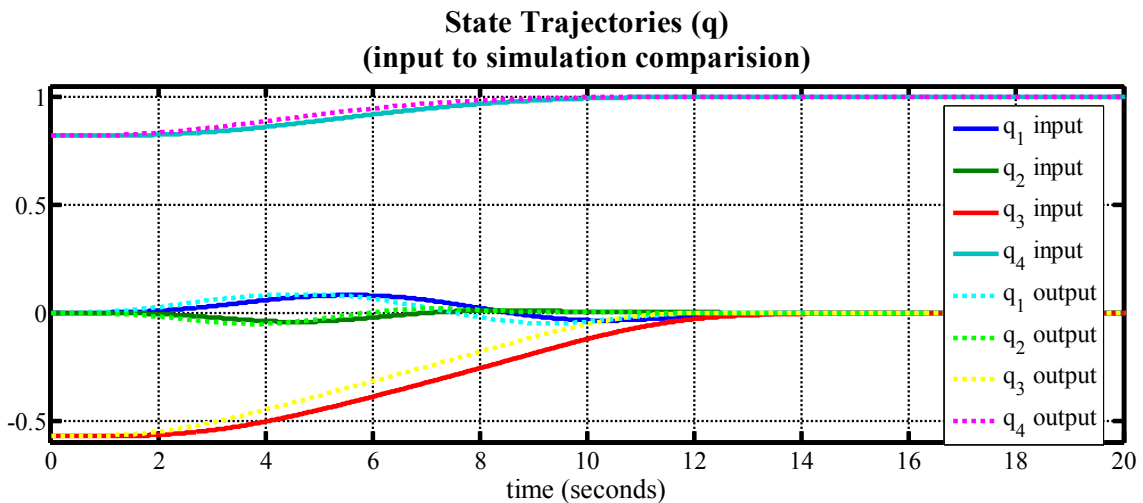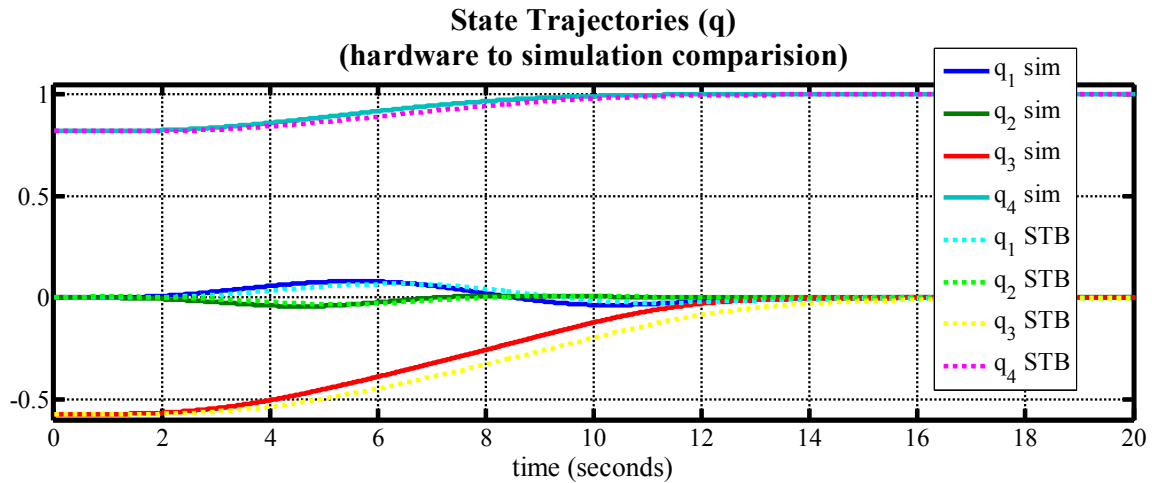

Figure 28.   Comparison of simulation output quaternions to hardware output quaternions.

Figure 28 reveals that the hardware response lags slightly behind the simulation. The causes of this lag were not investigated but likely reflect the imperfections in the model discussed above. This is reflected in an increased RMS error of 2.8193×10^{-2}.

The STB data includes most of the information needed to calculate the values of the individual terms. However, it is not instrumented to capture either gimbal acceleration or gimbal torque. This lack of data prevents calculation of Gimbal Term 2 and Rotor Term 3, however, these terms are assumed to be significant, therefore the inability to determine a relative magnitude is acceptable. The maximum relative magnitudes of each term were again calculated over the course of the simulation in the same manner as the closed loop analysis above.

Gimbal Term 1	Gimbal Term 2	Gimbal Term 3	Gimbal Term 4	Gimbal Term 5
$\mathbf{J}_g\left(\dfrac{d\left(\boldsymbol{\omega}^{b/N}\right)}{dt}\right)^g$	$\mathbf{J}_g\left(\dfrac{d\left(\boldsymbol{\omega}^{g/b}\right)}{dt}\right)^g$ Reduced Model	$\boldsymbol{\omega}^{b_g/N}\times\mathbf{J}_g\boldsymbol{\omega}^{b_g/N}$	$\boldsymbol{\omega}^{g/b}\times\mathbf{J}_g\boldsymbol{\omega}^{b/N}$	$\boldsymbol{\omega}^{b/N}\times\mathbf{J}_g\boldsymbol{\omega}^{g/b}$
100.0000%	Not Calculable	0.0000%	100.0000%	100.0000%
Gimbal Term 6	Rotor Term 1	Rotor Term 2	Rotor Term 3	Rotor Term 4
$\boldsymbol{\omega}^{g/b}\times\mathbf{J}_g\boldsymbol{\omega}^{g/b}$	$\mathbf{J}_r\left(\dfrac{d\left(\boldsymbol{\omega}^{b/N}\right)}{dt}\right)^g$	$\mathbf{J}_r\left(\dfrac{d\left(\boldsymbol{\omega}^{g/b}\right)}{dt}\right)^g$ Reduced Model	$\mathbf{J}_r\left(\dfrac{d\left(\boldsymbol{\omega}^{r/g}\right)}{dt}\right)^g$	$\boldsymbol{\omega}^{b_g/N}\times\mathbf{J}_r\boldsymbol{\omega}^{b_g/N}$
0.0000%	57.7567%	0.0000%	0.0000%	0.0000%
Rotor Term 5	Rotor Term 6	Rotor Term 7	Rotor Term 8	Rotor Term 9
$\boldsymbol{\omega}^{g/b}\times\mathbf{J}_r\boldsymbol{\omega}^{b/N}$	$\boldsymbol{\omega}^{b/N}\times\mathbf{J}_g\boldsymbol{\omega}^{g/b}$	$\boldsymbol{\omega}^{g/b}\times\mathbf{J}_g\boldsymbol{\omega}^{g/b}$	$\boldsymbol{\omega}^{b/N}\times\mathbf{J}_r\boldsymbol{\omega}^{r/g}$ Reduced Model	$\boldsymbol{\omega}^{g/b}\times\mathbf{J}_r\boldsymbol{\omega}^{r/g}$ Reduced Model
28.8784%	28.8784%	0.0000%	0.0000%	0.0000%

Table 12.   Maximum relative values for Gimbal and Rotor terms in Axis 1.

Gimbal Term 1	Gimbal Term 2	Gimbal Term 3	Gimbal Term 4	Gimbal Term 5
$\mathbf{J}_g \left(\dfrac{d\left(\boldsymbol{\omega}^{b/N}\right)}{dt} \right)^g$	$\mathbf{J}_g \left(\dfrac{d\left(\boldsymbol{\omega}^{g/b}\right)}{dt} \right)^g$ Reduced Model	$\boldsymbol{\omega}^{b_g/N} \times \mathbf{J}_g \boldsymbol{\omega}^{b_g/N}$	$\boldsymbol{\omega}^{g/b} \times \mathbf{J}_g \boldsymbol{\omega}^{b/N}$	$\boldsymbol{\omega}^{b/N} \times \mathbf{J}_g \boldsymbol{\omega}^{g/b}$
2.8131%	Not Calculable	0.0000%	0.028131%	0.028131%
Gimbal Term 6	Rotor Term 1	Rotor Term 2	Rotor Term 3	Rotor Term 4
$\boldsymbol{\omega}^{g/b} \times \mathbf{J}_g \boldsymbol{\omega}^{g/b}$	$\mathbf{J}_r \left(\dfrac{d\left(\boldsymbol{\omega}^{b/N}\right)}{dt} \right)^g$	$\mathbf{J}_r \left(\dfrac{d\left(\boldsymbol{\omega}^{g/b}\right)}{dt} \right)^g$ Reduced Model	$\mathbf{J}_r \left(\dfrac{d\left(\boldsymbol{\omega}^{r/g}\right)}{dt} \right)^g$	$\boldsymbol{\omega}^{b_g/N} \times \mathbf{J}_r \boldsymbol{\omega}^{b_g/N}$
0.0000%	0.008124%	0.0000%	0.0000%	0.007276%
Rotor Term 5	Rotor Term 6	Rotor Term 7	Rotor Term 8	Rotor Term 9
$\boldsymbol{\omega}^{g/b} \times \mathbf{J}_r \boldsymbol{\omega}^{b/N}$	$\boldsymbol{\omega}^{b/N} \times \mathbf{J}_g \boldsymbol{\omega}^{g/b}$	$\boldsymbol{\omega}^{g/b} \times \mathbf{J}_g \boldsymbol{\omega}^{g/b}$	$\boldsymbol{\omega}^{b/N} \times \mathbf{J}_r \boldsymbol{\omega}^{r/g}$ Reduced Model	$\boldsymbol{\omega}^{g/b} \times \mathbf{J}_r \boldsymbol{\omega}^{r/g}$ Reduced Model
0.016248%	0.008124%	0.0000%	100.0000%	100.0000%

Table 13.   Maximum relative values for Gimbal and Rotor terms in Axis 2.

Gimbal Term 1	Gimbal Term 2	Gimbal Term 3	Gimbal Term 4	Gimbal Term 5
$\mathbf{J}_g\left(\dfrac{d\left(\boldsymbol{\omega}^{b/N}\right)}{dt}\right)^g$	$\mathbf{J}_g\left(\dfrac{d\left(\boldsymbol{\omega}^{g/b}\right)}{dt}\right)^g$ Reduced Model	$\boldsymbol{\omega}^{b_g/N}\times\mathbf{J}_g\boldsymbol{\omega}^{b_g/N}$	$\boldsymbol{\omega}^{g/b}\times\mathbf{J}_g\boldsymbol{\omega}^{b/N}$	$\boldsymbol{\omega}^{b/N}\times\mathbf{J}_g\boldsymbol{\omega}^{g/b}$
0.0000%	Not Calculable	0.0000%	0.0000%	0.0000%
Gimbal Term 6	Rotor Term 1	Rotor Term 2	Rotor Term 3	Rotor Term 4
$\boldsymbol{\omega}^{g/b}\times\mathbf{J}_g\boldsymbol{\omega}^{g/b}$	$\mathbf{J}_r\left(\dfrac{d\left(\boldsymbol{\omega}^{b/N}\right)}{dt}\right)^g$	$\mathbf{J}_r\left(\dfrac{d\left(\boldsymbol{\omega}^{g/b}\right)}{dt}\right)^g$ Reduced Model	$\mathbf{J}_r\left(\dfrac{d\left(\boldsymbol{\omega}^{r/g}\right)}{dt}\right)^g$	$\boldsymbol{\omega}^{b_g/N}\times\mathbf{J}_r\boldsymbol{\omega}^{b_g/N}$
0.0000%	0.0000%	Not Calculable	0.0000%	0.008124%
Rotor Term 5	Rotor Term 6	Rotor Term 7	Rotor Term 8	Rotor Term 9
$\boldsymbol{\omega}^{g/b}\times\mathbf{J}_r\boldsymbol{\omega}^{b/N}$	$\boldsymbol{\omega}^{b/N}\times\mathbf{J}_g\boldsymbol{\omega}^{g/b}$	$\boldsymbol{\omega}^{g/b}\times\mathbf{J}_g\boldsymbol{\omega}^{g/b}$	$\boldsymbol{\omega}^{b/N}\times\mathbf{J}_r\boldsymbol{\omega}^{r/g}$ Reduced Model	$\boldsymbol{\omega}^{g/b}\times\mathbf{J}_r\boldsymbol{\omega}^{r/g}$ Reduced Model
0.0000%	0.0000%	0.0000%	100.0000%	0.0000%

Table 14.   Maximum relative values for Gimbal and Rotor terms in Axis 3.

Table 12, Table 13, and Table 14 confirm the results of the previous experimental analysis.

Section Notes

31 Mason A. Peck and Susan C. Kim, "New Results from the Spacecraft Momentum Control and Line-of-Sight Testbed," Advances in the Astronautical Sciences 118 (2004), 275.

32 Brian Underhill and Brian Hamilton, "Momentum Control System and Line-of-Sight Testbed (AAS 06-053)" (Advances in the Astronautical Sciences Guidance and Control, Breckenridge, CO, February 4-8, 2006), 554.

33 Ibid., 554.

34 Ibid., 554

THIS PAGE INTENTIONALLY LEFT BLANK

VI. CONCLUSIONS AND FUTURE WORK

A. CONCLUSIONS

The high fidelity model of a CMG controlled spacecraft results in a series of equations that significantly increase the complexity compared to current control models. The results from the verification and the experimental analysis show that the reduced model is highly accurate and can be successfully used to generate optimal path solutions. Specifically, the reduced model is accurate to greater than 0.01% in the gimbal torque axis. The closed loop analysis also reveals that several terms in the output axis may reach significance in certain cases. During closed loop testing the coupling terms between the angular velocity of the CMG and the angular velocity of the body $\left(\boldsymbol{\omega}^{g/b} \times \mathbf{J}_g \boldsymbol{\omega}^{b/N} \text{ and } \boldsymbol{\omega}^{b/N} \times \mathbf{J}_g \boldsymbol{\omega}^{g/b} \right)$ reach 1% relative value. With the addition of other, less significant terms, the total could reach 3% of the overall output torque. In the effort to maximize the ability to slew quickly and accurately, these terms may be exploitable.

B. FUTURE WORK

The current model is accurate in the steady state but inaccurate in the transient, best illustrated in Figure 17, and could be improved by including more aspects of the physical system, including friction terms and testbed imbalances. Specifically, the NPS testbed has an offset between its center of gravity and center of rotation. Including this offset in the model would increase the accuracy of the output.

While a large amount telemetry data is available from the Honeywell MCS, a more instrumented CMG / CMG table would increase the ability to determine when CMG back drive becomes significant and how it can avoided. This would also assist with increasing the accuracy of the model. All of this work could then be used to investigate how the high fidelity model could be used to calculate increased optimal solutions to the satellite slewing problem.

THIS PAGE INTENTIONALLY LEFT BLANK

LIST OF REFERENCES

Auclair, G. F. and R. C. Wells. "Control Moment Gyro Selection and Design Criteria." American Institute of Aeronautics and Astronautics, Guidance, Control and Flight Mechanics Conference, Santa Barbara, CA, August 17–19, 1970.

Bilimoria, Karl D. and Bong Wie. "Time-Optimal Three-Axis Reorientation of a Rigid Spacecraft." *Journal of Guidance Control Dynamics* 16, (1993): 452.

Burke, P. R. and P. A. Coronato. "A Gimbal Sizing Analysis for an IPACS Rotating Assembly." NASA Contractor Report #172524, (March, 1985).

Busseuil, Jacques, Michel Llibre, and Xavier Roser. "High Precision Mini-CMG's and their Spacecraft Applications." Advances in the Astronautical Sciences-Guidance and Control, Breckenridge, CO, February 4–8, 1998.

Cochran, J. E., B. K. Colburn, and N. O. Speakman. "Adaptive Spacecraft Attitude Control Utilizing Eigenaxis Rotations." American Institute of Aeronautics and Astronautics, Aerospace Sciences Meeting., Pasadena, CA, January 20–22, 1975.

Davis, Porter. "Momentum System Concepts and Trades for the New Class of Smaller Lower Cost Satellites." *Advances in the Astronautical Sciences* 125, (2006): 13–24.

Dzielski, John, Edward Bergmann, Joseph Paradiso, Derek Rowell, and David Wormley. "An Approach to CMG Steering using Feedback Linearization." NASA Contractor Report #183172, (1988).

Havill, Jerry R. and Jack W. Ratcliff. "A Twin-Gyro Attitude Control System for Space Vehicles." NASA Technical Note D-2419, (August, 1964).

Jacot, Arthur D. and Donald J. Liska. "Control Moment Gyros in Attitude Control." *Journal of Spacecraft and Rockets* (August, 1966): 1313–1320.

Jung, Dongwon and Panagiotis Tsiotras. "An Experimental Comparison of CMG Steering Control Laws." AIAA/AAS Astrodynamics Specialist Conference and Exhibit, Providence, RI, August 16–19, 2004.

Kennedy, H. B. "Gyro Momentum Exchange Device for Space Vehicle Attitude Control." *AIAA Journal* 1, no. 5 (May, 1963): 1110.

Kennel, Hans F. "Skylab Attitude Control and Angular Momentum Desaturation with One Double-Gimbaled Control Moment Gyro." NASA Technical Memorandum X- 64746, (1973).

Kolvek, J. M. "Advanced Control Moment Gyro Development [Final Summary Report]." NASA Contractor Report #120567, (1974).

Lappas, V., W. H. Steyn, and C. Underwood. "Design and Testing of a Control Moment Gyroscope Cluster for Small Satellites." *Journal of Spacecraft and Rockets* 42, no. 4 (July–Aug., 2005): 729-739.

Leonard, Barry S. *Control Moment Gyro Systems*. Vol. AE3818 Lecture Notes. Monterey, CA: 2002.

Leve, Frederick, Andrew Tatsch, and Norman Fitz-Coy. "A Scalable Control Moment Gyro Design for Attitude Control of Micro-, Nano-, and Pico-Class Satellites." *Advances in the Astronautical Sciences Guidance and Control 2007* 127, (2007): 235.

Messinger, Martin and Howard E. Parker. "The Dynamics of Gyroscope Damping for Geocentric Attitude Control." Air Force Office of Scientific Research Report PIBMRI-1147-63, (May, 1963).

Morine, L. A. and B. J. O'Connor. "A Description of the CMG and its Application to Space Vehicle Control." AIAA Guidance, Control And Flight Dynamics Conference, Huntsville, AL, August 14–16, 1969.

Morrell, Frederick R. "An Investigation of the Fine-Pointing Control System of a Soft Gimbaled Orbiting Telescope." NASA Technical Note D-5829, (1970).

Oh, H. S. and S. R. Vadali. "Maneuvering Strategies using CMGs." Flight Mechanics/Estimation Theory Symposium, Goddard Space Flight Center, Greenbelt, Maryland, May 10–11, 1988.

Peck, Mason A. and Susan C. Kim. "New Results from the Spacecraft Momentum Control and Line-of-Sight Testbed." *Advances in the Astronautical Sciences* 118, (2004): 1–16.

Richie, David J., Panagiotis Tsiotras, and J. L. Fausz. "Variable Speed Control Moment Gyroscope Workbench: A New Simulation Tool for Tomorrow's Spacecraft." Digital Avionics Systems Conference, 2001, Daytona Beach, FL, October 14–18, 2001.

Robertson, Brent P. and Michael L. Heck. "Space Station Attitude Control Momentum Requirements." American Institute of Aeronautics and Astronautics, Aerospace Sciences Meeting, Reno, NV, January 11–14, 1988.

Schaub, Hanspeter and John L. Junkins. *Analytical Mechanics of Space Systems*. AIAA Education Series. Reston, VA: American Institute of Aeronautics and Astronautics, 2003.

Schindelin, J. W. "On Space Vehicle Attitude Stabilization by Passive Control Moment Gyros." NASA Contractor Report #100280, (June, 1968).

Taniwaki, Shigemune and Yoshiaki Ohkami. "Precision Attitude Control of Spacecraft with Control Moment Gyros." AIAA Guidance, Navigation, and Control Conference Proceedings, Keystone, CO, August 21–24, 2006.

Thomas, Stephanie J., Michael A. Paluszek, and Mason Peck. "Architecture for Low-Power, High-Agility Multibody Control." AIAA Infotech@Aerospace, Arlington, VA, September 26–28, 2005.

Underhill, Brian and Brian Hamilton. "Momentum Control System and Line-of-Sight Testbed (AAS 06-053)." Advances in the Astronautical Sciences Guidance and Control, Breckenridge, CO, February 4–8, 2006.

Van Riper, R. "A Control Moment Gyro Fine Attitude Control System Final Technical Report " *United States* NASA Contractor Report #108702, (1970).

Wan, Jiuqing and Jiuqing Yu. "High Precision Satellite Attitude Control Based on Feedforward Compensation." The Sixth World Congress on Intelligent Control and Automation, Dalian, China, June 21–23, 2006.

Wie, Bong. "Quarternion Feedback Regulator for Spacecraft Eigenaxis Rotations." *Journal of Guidance, Control, and Dynamics* 12, (May–June, 1989): 375.

———. "Quaternion Feedback for Spacecraft Large Angle Maneuvers." *Journal of Guidance, Control and Dynamics* 8, no. 3 (May–June 1985, 1985): 360-365.

———. *Space Vehicle Dynamics and Control*. AIAA Education Series. 2nd ed. Reston, VA: American Institute of Aeronautics and Astronautics, 2008.

Wiesel, William E. *Spaceflight Dynamics* Mcgraw-Hill, 1997.

Winder, Lee and Sam Trundle. "3-DOF Satellite Simulator User's Guide." Andrews Space Document Number AS-5111-GUIDE-00001, (2009).

Yarber, G. W., A. F. Anderson, C. J. Bertrem, K. T. Chang, Joseph Kukel, B. F. McKee, C. S. Smith, and Sergel Tarhov. "Control Moment Gyro Optimization Study." NASA Contractor Report #400, (1966).

Yoon, Hyungjoo and Panagiotis Tsiotras. "Spacecraft Adaptive Attitude and Power Tracking with Variable Speed Control Moment Gyroscopes." *Journal of Guidance Control and Dynamics* 25, no. 6 (2002): 1081.

THIS PAGE INTENTIONALLY LEFT BLANK

INITIAL DISTRIBUTION LIST

1. Defense Technical Information Center
   Ft. Belvoir, Virginia

2. Dudley Knox Library
   Naval Postgraduate School
   Monterey, California

3. Head, Information Operations and Space Integration Branch,
   PLI/PP&O/HQMC,
   Washington, DC

4. Professor I. Michael Ross
   Naval Postgraduate School
   Monterey, California

5. Professor James H. Newman
   Naval Postgraduate School
   Monterey, California

6. CDR Christine McManus
   Naval Postgraduate School
   Monterey, California